Conductive and viscous sub-layers on forced convection and mechanism of critical heat flux during flow boiling of subcooled water in a platinum circular tube with 3 mm inner diamete…

Hata, K.

Liu, Q. S.

(Citation)
International Journal of Heat and Mass Transfer,162:120269

(Issue Date)
2020-12

(Resource Type)
journal article

(Version)
Accepted Manuscript

(URL)
https://hdl.handle.net/20.500.14094/90007664

Conductive and viscous sub-layers on forced convection and Mechanism of critical heat flux during flow boiling of subcooled water in a Platinum circular tube with 3 mm inner diameter and 32.7 mm heated length at high liquid Reynolds number

K. Hata* and Q.S. Liu

Graduate School of Maritime Sciences, Kobe University

5-1-1, Fukaeminami, Higashinada, Kobe 658-0022, Japan

hatako1@people.kobe-u.ac.jp; qsliu@maritime.kobe-u.ac.jp

ABSTRACT

The turbulent heat transfer, the subcooled boiling heat transfer and the steady state CHF for a Pt-circular test tube of a 3 mm inner diameter and a 32.7 mm heated length are measured with a wide range of inlet subcooling and flow velocity at high liquid Reynolds number, i.e. Re_d=2.35×10^4 to 1.12×10^5. For flow velocities ranging from 4.103 to 21.446 m/s, the inner surface temperature of the Pt circular test tube calculated by the steady one-dimensional heat conduction equation is compared with the value obtained from our turbulent heat transfer correlation equation and the numerical solution of the RANS equation (Reynolds mean Navier-Stokes simulation) of the k-ε turbulence model. The conduction sub-layer thicknesses from the non-boiling region to CHF are measured in the conduction sub-layer itself in the forced convection region and the thinner sub-layer dissipated by boiling evaporation in the nucleate boiling region. The nondimensional thicknesses of local and average conductive sub-layers and, the thicknesses and nondimensional thicknesses of local and average viscous sub-layers on forced convection are estimated from the thicknesses of local and average conductive sub-layers and Prandtl numbers evaluated at the calculated temperature of the first control volume on the heated surface. In addition, the thickness of the conductive

* Corresponding author.

sublayer at the CHF point is estimated from measurements at various flow velocities. The experimental values of the CHF are also compared with authors' widely and precisely predictable correlations of critical heat flux during flow boiling of subcooled water and the corresponding theoretical values of the liquid sub-layer dry-out models suggested by other researchers, respectively. The authors' correlations and other researchers' theoretical values can represent the subcooled boiling CHFs obtained in this study within the ranges of -22.74 to -6.21% difference and -22.17 to 6.16 % one, respectively. Proposals for the main mechanism of critical heat flux during flow boiling of subcooled water on vertical tubes are confirmed again at high liquid Reynolds numbers based on experimental data. The boiling transitions to film boiling at the subcooled water flow boiling in the Pt test tube of d=3 mm and L=32.7 mm is not due to heterogeneous spontaneous nucleation or hydro-dynamic instability, but to **liquid sub-layer dry-out model** at the steady-state CHF. It is similar to those for the Pt test tubes with d=3 mm and L=66.5 mm, and d=3 mm and L=100 mm.

KEYWORDS

Conductive sub-layer, Viscous sub-layer, Prandtl number, Mechanism of critical heat flux, Circular tube, High liquid Reynolds number, Liquid sub-layer dry-out model

1. INTRODUCTION

The knowledge of turbulent heat transfer and subcooled boiling heat transfer at high liquid Reynolds number is important to discuss the conductive and viscous sub-layers and the mechanisms of subcooled flow boiling critical heat flux (CHF) in a vertical circular tube. Many researchers have experimentally studied the steady state CHFs, $q_{cr,sub,st}$, uniformly heated on the normal tubes by a steadily increasing current for high liquid Reynolds number and given the correlations for calculating CHFs on the normal tubes. It has been clarified that the $q_{cr,sub,st}$ against $\Delta T_{sub,out}$ for $\Delta T_{sub,out}$≥30 K are almost proportional to $d^{-0.4}$ and $u^{0.4}$ for fixed $\Delta T_{sub,out}$ and L/d, to $(\Delta T_{sub,out})^{0.7}$ for a fixed L/d and to $(L/d)^{-0.1}$ for a fixed $\Delta T_{sub,out}$. And, the $q_{cr,sub,st}$ are also proportional to $u^{0.55}$ for the experimental data at u>13.3 m/s. The authors have given the steady-state CHF correlations against outlet and inlet subcoolings based on the effects of test tube inner diameter (d), flow velocity (u),

outlet and inlet subcoolings ($\Delta T_{sub,out}$ and $\Delta T_{sub,in}$) and ratio of heated length to inner diameter (L/d) on CHF [1-11]. It has been assumed that flow velocity will affect the incipient boiling superheat and the nucleate boiling heat transfer up to the CHF. Incipient boiling superheat may shift to a very high value at higher flow velocity and a direct transition to film boiling or a trend of a decrease in CHF with an increase in the flow velocity may occur due to the heterogeneous spontaneous nucleation [9-12] but not due to the hydro-dynamic instability [13, 14] or the liquid sublayer dry-out model [15-17]. To clarify the change in CHF generation mechanism, accurate experimental measurement of subcooled boiling heat transfer up to CHF is required.

The purpose of the current research is fivefold. First is to measure the turbulent heat transfer, the subcooled boiling heat transfer and the steady state CHFs for a Pt-circular test tube of a 3 mm inner diameter and a 32.7 mm heated length with a wide range of inlet subcoolings ($\Delta T_{sub,in}$) and flow velocities (u) at high liquid Reynolds number. Second is to compare the inner surface temperature of the Pt-circular test tube calculated by the steady one-dimensional heat conduction equation with the turbulent heat transfer correlation for the flow velocities ranging from 4.103 to 21.206 m/s. Third is to estimate the nondimensional thicknesses of local and average conductive sub-layers and, the thicknesses and nondimensional thicknesses of local and average viscous sub-layers on forced convection from the thicknesses of local and average conductive sub-layers and Prandtl numbers evaluated at the calculated temperature of the first control volume on the heated surface. Fourth is to measure the thicknesses of conductive sub-layer from non-boiling regime to CHF by numerically analyzing the subcooled flow boiling heat transfer on a Pt-circular test tube of a 3 mm inner diameter and a 32.7 mm heated length. Fifth is to confirm again proposals for the main mechanism of critical heat flux during flow boiling of subcooled water on vertical tubes at high liquid Reynolds numbers based on experimental data.

2. EXPERIMENTAL APPARATUS AND METHOD

The schematic diagram of the experimental setup comprised of a water loop and a pressurizer is shown in Fig. 1. The loop is made of SUS304 stainless steel and is capable of working up to 2 MPa. The loop has five

test sections with inner diameters of 2, 3, 6, 9, and 12 mm. The test section is oriented vertically to allow the water to flow upward. For this work, a 3 mm inner diameter test section was used.

Figure 2 shows a cross-sectional view of the 3 mm inner diameter test section used. For this work, a 3 mm inner diameter test tube inner diameter (d), a 32.7 mm heated length (L), and a commercially available internally finished (CF) for platinum (Pt) test tube was used. The wall thickness of the test tube (δ) was 0.5 mm. 5 mm thick silver-plated copper electrode plates to supply the heating current were soldered to the surfaces at both ends of the test tube. The ends of the test tube were electrically isolated from the loop by a 14 mm thick Bakelite plates. The inner surface of the test tube was observed with a scanning electron microscope（SEM) photograph and inner surface roughness was measured by the surface texture measuring instrument (SURFCOM 120A) of Tokyo Seimitsu Co., Ltd., (Mitaka, Tokyo, Japan). Figure 3 shows the result of SEM photograph of the inner surface of platinum (Pt) test tube of d=3 mm with the commercial finish of inner surface. The inner surface roughness is measured 0.40 μm for average roughness, *Ra*, 2.20 μm for maximum roughness depth, *Rmax*, and 1.50 μm for mean roughness depth, *Rz*.

The platinum (Pt) test tube has been heated with an exponentially increasing heat input supplied from a direct current source (Takasago Ltd., Kawasaki, Kanagawa, Japan, NL035-500R, DC 35 V-3000 A) through the two copper electrodes shown in Fig. 4. Heat transfer process caused by a exponentially increasing heat input, $Q_0 \exp(t/\tau)$, were measured for the platinum test tube. The exponential periods, τ, of the heat input ranged from 7.79 s to 25.95 s. In CHF, the average temperature of the test tube rises rapidly. When the measured average temperature rose to the preset temperature, the heat input to the test tube was automatically shut off, which was several degrees (in tens) of Kelvin higher than corresponding CHF surface temperature. This procedure avoided the actual burning of the test tube.

The average temperature, $\bar{T}$, of the Pt test tube shown in Fig. 4 was measured with resistance thermometry participating as a branch of a double bridge circuit for the temperature measurement. The output voltage, V_T, from the bridge circuit and the voltage drops of the test tube potential taps and standard resistance, $V_R=IR_T$

and $V_I = IR_s$, were amplified and sent to a digital computer via an analog-to-digital (A/D) converter. The unbalanced voltage, V_T, is expressed by Ohm's law in the form:

$$V_T = \frac{I(R_T \times R_2 - R_1 \times R_3)}{R_2 + R_3} \quad (1)$$

These voltages were sampled simultaneously at regular intervals ranging from 60 ms to 200 ms. The average temperatures of the Pt test tube between the potential taps were calculated with the aid of previously calibrated resistance-temperature relation, $R_T = a(1 + b\bar{T} + c\bar{T}^2)$. The coefficients of the circular test tube THD173 used in this study are as follows. a = 0.61349012 mΩ, b =0.0038980686, c = -0.000000588. The heat generation rates of the Pt test tube between the potential taps, $Q = I^2 R_T$, were calculated from the measured voltage difference between the potential taps of the Pt test tube, V_R, and that across the standard resistance, V_I. The surface heat flux between the potential taps, q, is the differences between the heat generation rate per unit volume, Q, and the rate of change of energy storage in the Pt test tube obtained from the faired average temperature versus time curve as follows:

$$q = \frac{V}{S}\left(Q - \rho c \frac{d\bar{T}}{dt}\right) \quad (2)$$

where ρ, c, V, and S are the density, specific heat, volume, and inner surface area of the Pt tube, respectively.

The heater inner surface temperatures between the potential taps, T_s, were also obtained by solving a steady one-dimensional heat conduction equation in a test tube under the conditions of the measured average temperature, $\bar{T}$, and the surface heat flux of the test tube, q. The solutions of the inner and outer surface temperatures, T_s and T_{so}, of the test tube are given by a steady one-dimensional heat conduction equation. The basic formula for a test tube is:

$$\frac{d^2T}{dr^2} + \frac{1}{r}\frac{dT}{dr} + \frac{Q}{\lambda} = 0 \quad (3)$$

then, the integrated yield and the average tube temperature are obtained.

$$T(r) = -\frac{Qr^2}{4\lambda} + \frac{Qr_o^2}{2\lambda} \ln r + C \quad (4)$$

$$\bar{T} = \frac{1}{\pi(r_o^2 - r_i^2)} \int_{r_i}^{r_o} 2\pi r T(r) dr \quad (5)$$

The generation of heat in the tube is equivalent to heat conduction, and the test tube is completely insulated.

$$q = -\lambda \left.\frac{dT}{dr}\right|_{r=r_i} = \frac{\left(r_o^2 - r_i^2\right)Q}{2r_i} \tag{6}$$

$$\left.\frac{dT}{dr}\right|_{r=r_o} = 0 \tag{7}$$

The temperature of the inner and outer surfaces of the heater, T_s and T_{so}, and C in Eq. (4) can be explained as follows.

$$T_s = T(r_i) = \overline{T} - \frac{qr_i}{4(r_o^2 - r_i^2)^2\lambda}\left[4r_o^2\left\{r_o^2\left(\ln r_o - \frac{1}{2}\right) - r_i^2\left(\ln r_i - \frac{1}{2}\right)\right\} - \left(r_o^4 - r_i^4\right)\right] - \frac{qr_i}{2(r_o^2 - r_i^2)\lambda}\left(r_i^2 - 2r_o^2 \ln r_i\right) \tag{8}$$

$$T_{so} = T(r_o) = \overline{T} - \frac{qr_i}{4(r_o^2 - r_i^2)^2\lambda}\left[4r_o^2\left\{r_o^2\left(\ln r_o - \frac{1}{2}\right) - r_i^2\left(\ln r_i - \frac{1}{2}\right)\right\} - \left(r_o^4 - r_i^4\right)\right] - \frac{qr_i r_o^2}{2(r_o^2 - r_i^2)\lambda}\left(1 - 2\ln r_o\right) \tag{9}$$

$$C = \overline{T} - \frac{qr_i}{4(r_o^2 - r_i^2)^2\lambda}\left[4r_o^2\left\{r_o^2\left(\ln r_o - \frac{1}{2}\right) - r_i^2\left(\ln r_i - \frac{1}{2}\right)\right\} - \left(r_o^4 - r_i^4\right)\right] \tag{10}$$

where $\overline{T}$, q, λ, r_i, and r_o are the average tube temperature, heat flux, thermal conductivity, inner tube radius, and outer tube radius, respectively.

The inlet and outlet pressures, P_{in} and P_{out}, for the 3 mm inner diameter test section were calculated from the pressures measured by inlet and outlet pressure transducers, P_{ipt} and P_{opt}, as follows:

$$P_{in} = P_{ipt} - \left\{\left(P_{ipt}\right)_{wnh} - \left(P_{opt}\right)_{wnh}\right\} \times \frac{L_{ipt}}{L_{ipt} + L + L_{opt}} \tag{11}$$

$$P_{out} = P_{in} - \left(P_{in} - P_{opt}\right) \times \frac{L}{L + L_{opt}} \tag{12}$$

where L_{ipt} = 0.053 m and L_{opt} = 0.053 m for 3 mm ID. The experimental errors are estimated to be ± 1 K at the inner tube surface temperature and ± 2% at the heat flux. Mass velocity, inlet and outlet sub-coolings, inlet and outlet pressures, and exponential period were measured with errors within ± 2%, ± 1K, ± 4kPa, and ± 2%, respectively.

3. NUMERICAL SOLUTION OF TURBULENT HEAT TRANSFER

3.1. RANS equations for k-ε turbulence model with high Reynolds number form

The RANS equations for k-ε turbulence model [18] in a circular tube of 3 mm in diameter and 492 mm long were numerically solved for heating of water with heated section of 3 mm in diameter and 33 mm long by using PHOENICS code under the same conditions as the experimental ones and with temperature dependent thermo-physical fluid properties [19]. The unsteady RANS equations for turbulent heat transfer are solved in the three dimensional coordinate shown in Fig. 5 as follows [20].

(Continuity Equation) Cylindrical coordinates (r, θ, z):

$$\frac{\partial \rho}{\partial t}+\frac{1}{r}\frac{\partial}{\partial r}(ru_r\rho)+\frac{1}{r}\frac{\partial}{\partial \theta}(u_\theta\rho)+\frac{\partial}{\partial z}(u_z\rho)=0 \tag{13}$$

(Momentum Equation) Cylindrical coordinates (r, θ, z)

r-component:

$$\frac{\partial}{\partial t}(\rho u_r)+\frac{\partial}{\partial r}(\rho u_r u_r)+\frac{1}{r}\frac{\partial}{\partial \theta}(\rho u_\theta u_r)-\frac{\rho u_\theta^2}{r}+\frac{\partial}{\partial z}(\rho u_z u_r)=-\frac{\partial P}{\partial r}+\frac{1}{r}\frac{\partial}{\partial r}\left(r\tau_{rr}\right)+\frac{1}{r}\frac{\partial}{\partial \theta}\tau_{r\theta}-\frac{\tau_{\theta\theta}}{r}+\frac{\partial}{\partial z}\tau_{rz}+\rho g_r \tag{14}$$

θ-component:

$$\frac{\partial}{\partial t}(\rho u_\theta)+\frac{\partial}{\partial r}(\rho u_r u_\theta)+\frac{1}{r}\frac{\partial}{\partial \theta}(\rho u_\theta u_\theta)+\frac{\rho u_r u_\theta}{r}+\frac{\partial}{\partial z}(\rho u_z u_\theta)=-\frac{1}{r}\frac{\partial P}{\partial \theta}+\frac{1}{r^2}\frac{\partial}{\partial r}\left(r^2\tau_{r\theta}\right)+\frac{1}{r}\frac{\partial}{\partial \theta}\tau_{\theta\theta}+\frac{\partial}{\partial z}\tau_{\theta z}+\rho g_\theta \tag{15}$$

z-component:

$$\frac{\partial}{\partial t}(\rho u_z)+\frac{\partial}{\partial r}(\rho u_r u_z)+\frac{1}{r}\frac{\partial}{\partial \theta}(\rho u_\theta u_z)+\frac{\partial}{\partial z}(\rho u_z u_z)=-\frac{\partial P}{\partial z}+\frac{1}{r}\frac{\partial}{\partial r}\left(r\tau_{rz}\right)+\frac{1}{r}\frac{\partial}{\partial \theta}\tau_{\theta z}+\frac{\partial}{\partial z}\tau_{zz}+\rho g_z \tag{16}$$

(Energy Equation) Cylindrical coordinates (r, θ, z):

$$\begin{aligned}&\rho\frac{\partial h}{\partial t}+\rho\frac{\partial}{\partial r}(u_r h)+\rho\frac{1}{r}\frac{\partial}{\partial \theta}(u_\theta h)+\rho\frac{\partial}{\partial z}(u_z h)=\\&\frac{1}{r}\frac{\partial}{\partial r}\left\{\left(\lambda+c_p\frac{\mu_t}{\sigma_t}\right)r\frac{\partial T}{\partial r}\right\}+\frac{1}{r^2}\frac{\partial}{\partial \theta}\left\{\left(\lambda+c_p\frac{\mu_t}{\sigma_t}\right)\frac{\partial T}{\partial \theta}\right\}+\frac{\partial}{\partial z}\left\{\left(\lambda+c_p\frac{\mu_t}{\sigma_t}\right)\frac{\partial T}{\partial z}\right\}+Q\end{aligned} \tag{17}$$

(Transport Equation for k) Cylindrical coordinates (r, θ, z):

$$\begin{aligned}&\rho\frac{\partial k}{\partial t}+\rho\frac{\partial}{\partial r}(u_r k)+\rho\frac{1}{r}\frac{\partial}{\partial \theta}(u_\theta k)+\rho\frac{\partial}{\partial z}(u_z k)=\\&\frac{1}{r}\frac{\partial}{\partial r}\left\{\left(\mu+\frac{\mu_t}{\sigma_k}\right)r\frac{\partial k}{\partial r}\right\}+\frac{1}{r^2}\frac{\partial}{\partial \theta}\left\{\left(\mu+\frac{\mu_t}{\sigma_k}\right)\frac{\partial k}{\partial \theta}\right\}+\frac{\partial}{\partial z}\left\{\left(\mu+\frac{\mu_t}{\sigma_k}\right)\frac{\partial k}{\partial z}\right\}+\rho(P_k+\Gamma_b-\varepsilon)\end{aligned} \tag{18}$$

(Transport Equation for ε) Cylindrical coordinates (r, θ, z):

$$\begin{aligned}&\rho\frac{\partial \varepsilon}{\partial t}+\rho\frac{\partial}{\partial r}(u_r \varepsilon)+\rho\frac{1}{r}\frac{\partial}{\partial \theta}(u_\theta \varepsilon)+\rho\frac{\partial}{\partial z}(u_z \varepsilon)=\\&\frac{1}{r}\frac{\partial}{\partial r}\left\{\left(\mu+\frac{\mu_t}{\sigma_\varepsilon}\right)r\frac{\partial \varepsilon}{\partial r}\right\}+\frac{1}{r^2}\frac{\partial}{\partial \theta}\left\{\left(\mu+\frac{\mu_t}{\sigma_\varepsilon}\right)\frac{\partial \varepsilon}{\partial \theta}\right\}+\frac{\partial}{\partial z}\left\{\left(\mu+\frac{\mu_t}{\sigma_\varepsilon}\right)\frac{\partial \varepsilon}{\partial z}\right\}+\rho\frac{\varepsilon}{k}(C_{1e}P_k+C_{3e}\Gamma_b-C_{2e}\varepsilon)\end{aligned} \tag{19}$$

where $\tau_{rr} = 2\rho\nu\frac{\partial u_r}{\partial r}$ (20)

$$\tau_{\theta\theta} = 2\rho\nu\left(\frac{1}{r}\frac{\partial u_\theta}{\partial \theta} + \frac{u_r}{r}\right) \quad (21)$$

$$\tau_{zz} = 2\rho\nu\frac{\partial u_z}{\partial z} \quad (22)$$

$$\tau_{r\theta} = \tau_{\theta r} = \rho\nu\left(r\frac{\partial}{\partial r}\left(\frac{u_\theta}{r}\right) + \frac{1}{r}\frac{\partial u_r}{\partial \theta}\right) \quad (23)$$

$$\tau_{\theta z} = \tau_{z\theta} = \rho\nu\left(\frac{\partial u_\theta}{\partial z} + \frac{1}{r}\frac{\partial u_z}{\partial \theta}\right) \quad (24)$$

$$\tau_{zr} = \tau_{rz} = \rho\nu\left(\frac{\partial u_z}{\partial r} + \frac{\partial u_r}{\partial z}\right) \quad (25)$$

$$g_r = 0,\ g_\theta = 0,\ g_z = -g \quad (26)$$

$$h = c_p T \quad (27)$$

$$\nu_t = C_\mu \frac{k^2}{\varepsilon} \quad (28)$$

$$P_k = \nu_t\left[2\left\{\left(\frac{\partial u_r}{\partial r}\right)^2 + \left(\frac{1}{r}\frac{\partial u_\theta}{\partial \theta} + \frac{u_r}{r}\right)^2 + \left(\frac{\partial u_z}{\partial z}\right)^2\right\} + \left(\frac{1}{r}\frac{\partial u_r}{\partial \theta} + \frac{\partial u_\theta}{\partial r} - \frac{u_\theta}{r}\right)^2 + \left(\frac{\partial u_\theta}{\partial z} + \frac{1}{r}\frac{\partial u_z}{\partial \theta}\right)^2 + \left(\frac{\partial u_z}{\partial r} + \frac{\partial u_r}{\partial z}\right)^2\right] \quad (29)$$

$$\Gamma_b = \frac{-\nu_t}{\rho\sigma_t}\left(g_r\frac{\partial \rho}{\partial r} + g_\theta\frac{1}{r}\frac{\partial \rho}{\partial \theta} + g_z\frac{\partial \rho}{\partial z}\right) \quad (30)$$

$$\lambda_e = \lambda_t + \lambda \quad (31)$$

$$\lambda_t = \frac{c_p\mu_t}{\sigma_t} \quad (32)$$

$$\nu = \frac{\mu}{\rho} + \nu_t \quad (33)$$

u_r, u_θ and u_z are the r, θ and z components of a velocity vector, respectively. The constants, σ_k, σ_ε, σ_t, C_{1e}, C_{2e}, C_{3e} and C_μ, appearing in the unsteady RANS equations for turbulent heat transfer take the values given in Table 1 [20].

3.2. Boundary conditions

The basic equations are analyzed numerically with the following boundary conditions:

Outer boundary of heated section: constant heat flux and non-slip condition.

$$q = -\lambda \frac{\partial T}{\partial r} = constant \tag{34}$$

At the outer boundary of non-heated section:

$$\frac{\partial T}{\partial r} = 0 \tag{35}$$

At the lower boundary:

$$T = T_{in}, \quad u_r = 0, \quad u_\theta = 0 \quad and \quad u_z = u \qquad \text{for inflow} \tag{36}$$

where T_{in} and u are an inlet liquid temperature and a flow velocity at the entrance of the test section.

3.3. Method of solution

The control volume discretization equations were derived from these basic equations using a hybrid scheme [21]. The thermo-physical properties for each control volume are given by each control volume temperature numerically analyzed. The procedure for calculating the flow field is the SIMPLE algorithm, which represents the semi-implicit solution of the pressure-association equation [22]. A uniform heat flux, q, was prescribed at the heated circular tube wall for the range of 2.628×10^5 W/m^2 to 4.930×10^7 W/m^2 as a boundary condition, and numerical calculations continued until a steady state was obtained. The local surface temperature on the test tube, T_s, was analyzed from the calculated temperature of the first control volume on the test tube surface, *TEM*, which is located on the center of the control volume, by solving the heat conduction equation in liquid as follows [23-29].

$$T_s = \frac{q}{\lambda_l} \frac{(\Delta r)_{out}}{2} + TEM \tag{37}$$

where, $(\Delta r)_{out}$ is the first control volume width on the r-component. In Fig. 6, the test tube surface is located at r=-1.5 mm and the conductive sub-layer [23-29] exists on the test tube surface. The liquid temperatures in the conductive sub-layer on the test tube surface will become linearly lower with a decrease in the radius by the heat conduction from the surface temperature on the test tube, $T_f=T_s-q(\Delta r)_{out}/2\lambda_l$. And let those, T_f, equal the calculated liquid temperature of the outer control volume on the test tube surface, *TEM*, in the turbulent flow region, which is located on the center of the control volume as given in Eq. (37). Half of the outer

control volume width of the r component, $(\Delta r)_{out} / 2$, will be the thickness of the conductive sublayer, δ_{CSL}, for the turbulent heat transfer in a circular tube under two-phase model classified into conductive sub-layer and inner region of the turbulent flow [23-27]. Average heat transfer coefficient on the test tube surface was obtained by $T_{s,av}$ averaging the calculated local surface temperatures, T_s, at every 0.25 mm in the heated length, L. The flow and temperature field predictions were obtained using the PHOENICS CFD code [19].

4. RESULTS AND DISCUSSION

4.1. Experimental conditions and parameters used for calculation

Steady-state heat transfer processes on the Pt test tube of 3 mm inner diameter and a 32.7 mm heated length that caused by the exponentially increasing heat inputs, $Q_0 exp(t/\tau)$, were measured. Exponential periods, τ, of heat input ranged from 7.79 s to 25.95 s. Initial experimental conditions such as inlet flow velocity, inlet liquid temperature, inlet pressure and exponential period for the CHF experiment were determined independent of each other before each experimental run.

The experimental conditions are as follows.

Test Tube Number	THD-F173
Heater material	platinum
Surface condition	Commercial finish of inner surface (CF)
Surface roughness	0.40 μm for *Ra*, 2.20 μm for *Rmax* and 1.50 μm for *Rz*
Inner diameter (d)	3 mm
Heated length (L)	32.7 mm
L/d	10.9
Wall thickness (δ)	0.5 mm
Inlet flow velocity (u)	4.222, 7.314, 10.407, 13.715, 17.340 and 21.446 m/s on forced convection 4.103, 7.076, 10.129, 13.428, 17.146 and 21.206 m/s at CHF
Liquid Reynolds numbers (Re_d)	2.35×10^4 to 1.12×10^5
Inlet pressure (P_{in})	831.51 to 942.94 kPa
Outlet pressure (P_{out})	817.99 to 872.39 kPa
Inlet subcooling ($\Delta T_{sub,in}$)	134.70 to 140.79 K
Outlet subcooling ($\Delta T_{sub,out}$)	94.34 to 119.51 K
Inlet liquid temperature (T_{in})	308.20 to 311.28 K
Exponentially increasing heat input (Q)	$Q_0 exp(t/\tau)$, τ=7.79 to 25.95 s

The parameters used for calculation were as follows:

Inner diameter (d)	3 mm
Heated length (L)	33 mm
Entrance length (L_e)	282 mm
Exit length (L_{ex})	177 mm
Test section length (L_{ts})	492 mm
Heat flux (q)	2.628×10^5 to 4.930×10^7 W/m^2 ($q_0\,exp(t/\tau)$, τ=23.52 to 25.95 s)
Inlet flow velocity (u)	4.222, 7.314, 10.407, 13.715, 17.340 and 21.446 m/s on forced convection 4.103, 7.076, 10.129, 13.428, 17.146 and 21.206 m/s at CHF
Liquid Reynolds numbers (Re_d)	2.35×10^4 to 1.12×10^5
Inlet liquid temperature (T_{in})	308.20 to 311.28 K
Coordinate system	cylindrical coordinate (r, θ, z)
Control volume number	(20 to 45, 60, 894)
Physical model	k-ε turbulence model with high Reynolds number form
Wall functions	logarithmic law ($7.2174\leq y^+_{CSL,av}\leq19.9446$)

4.2. Steady state heat transfer characteristics

4.2.1. Heat transfer curve

Figure 7 has been shown typical example of the heat transfer curves for the exponential period, τ, of around 25 s on the Platinum test tube of d=3 mm and L=32.7 mm at the inlet liquid temperature, T_{in}, of around 308.38 K and the flow velocities, u, of 4 to 21 m/s. At a constant flow velocity, the heat flux gradually increases with increasing ΔT_{sat} ($=T_s$-T_{sat}) on the non-boiling forced convection curve derived from the correlation, Eq. (38), [30] until the point where the heat flux begins to increase the gradient at the onset of nucleate boiling.

$$Nu_d = 0.02\,Re_d^{0.85}\,Pr^{0.4}\left(\frac{L}{d}\right)^{-0.08}\left(\frac{\mu}{\mu_w}\right)^{0.14} \tag{38}$$

All properties of the equation are evaluated at the average bulk liquid temperature, T_L, [$=(T_{in}+(T_{out})_{cal})/2$], except μ_w, which is evaluated at the heater inner surface temperature. And the heat flux increases up to the CHF where the heater surface temperature rapidly jumps from the nucleate boiling heat transfer regime to the film boiling one. The CHF and its superheat become higher with an increase in flow velocity. The nucleate boiling curves in higher heat flux range for each flow velocity agree with each other forming a single straight line on the $log\ q$ versus $log\ \Delta T_{sat}$ graph. The fully developed subcooled boiling curve for

Platinum test tube with a commercial finish of inner surface can be expressed by the following empirical correlation.

$$q = C\Delta T_{sat}^{n} = 1630\Delta T_{sat}^{3} \tag{39}$$

where C and n are coefficient and exponent, and equivalent to 1630 and 3 respectively. The correlation can almost describe the fully developed subcooled boiling curves for the Platinum test tube of d=3 mm and L=32.7 mm with the commercial finish of inner surface at the outlet pressure of around 800 kPa obtained in this work within 15 % difference under the wide range of flow velocities. The corresponding curve derived from the correlation, Eq. (40) with C_{sf}=0.0094 for fully developed subcooled boiling given by Rohsenow [31] is also shown in Fig. 7 for comparison.

$$\frac{c_{pl}\Delta T_{sat}}{h_{fg}} = C_{sf}\left(\frac{q}{\mu_l h_{fg}}\sqrt{\frac{\sigma}{g(\rho_l-\rho_g)}}\right)^{0.33}\left(\frac{c_{pl}\mu_l}{\lambda_l}\right)^{1.7} \tag{40}$$

where, various fluid properties are evaluated at the saturation temperature corresponding to the local pressure, and C_{sf} is a function of the particular heated surface and fluid combination. The value calculated from the correlation is in good agreement with the corresponding value of the Rohsenow correlation, Eq. (40), at C_{sf} = 0.0094 in the log q vs. log T_{sat} graph. The values of the lower limit of the heterogeneous spontaneous nucleation temperature, T_{HET}, [12] and the homogeneous spontaneous nucleation temperature, T_H, [32] at 800 kPa are shown below the figure. The tube inner surface temperature in CHF at a flow velocity of 21 m / s is 51.90 K and 106.62 K lower than T_{HET} and T_H, respectively.

4.2.2. Thickness and nondimensional thickness of local conductive sub-layer, δ_{CSL} and y^+_{CSL}, on forced convection

Figures 8, 9 and 10 show the experimental results of average inner surface temperature ($T_{s,av}$-black solid circle), heat flux (q-black solid line) and, inlet and outlet liquid temperatures (T_{in} and T_{out}-black solid squares) against the z-axis distance from the leading edge of the heated section at the flow velocities, u, of 13.64,13.67 and 13.71 m/s with the heat fluxes, q, of 3.009, 5.176 and 8.906 MW/m^2, respectively. The liquid temperatures are linearly estimated from the values of the inlet liquid temperature, T_{in}, and outlet ones,

T_{out}. The average inner surface temperature ($T_{s,av}$) was obtained from Eq. (8) using the measured average temperature of the Pt tube and the surface heat flux.

The numerical solutions of the *z*-axis variations in the analyzed liquid temperature of the outer control volume on the test tube surface, *TEM*, are shown at the heat fluxes of 3.043, 5.098 and 8.541 MW/m^2 with the flow velocities of 13.71 m/s as a green 1-dot dashed line in each figure. The numerical solutions of the local inner surface temperatures on the test tube, T_s, were calculated from the analyzed liquid temperature of the outer control volume on the test tube surface, *TEM*, which is located on the center of the control volume, by solving the liquid heat conduction equation given by Eq. (37). The *z*-axis variations in the inner surface temperature of the test tube at every 0.25 mm in the heated length, *L*, are shown as green solid line in the figure. They become gradually higher with an increase in the *z*-axis distance from the leading edge of the heated section. The average values of numerical solution of the local inner surface temperature ($T_{s,av}$-green solid circle) solved by the theoretical equations for turbulent heat transfer, Eqs. (13) to (36), almost agree with the experimental results ($T_{s,av}$-black solid circle) given by Eq. (8) which are obtained from the steady one-dimensional heat conduction equation within +7.30 % difference. The thickness of the local conductive sub-layer, δ_{CSL}, for the turbulent heat transfer on the Pt test tube of d=3 mm and L=32.7 mm is 6.52 μm at the heat fluxes of 3.043, 5.098 and 8.541 MW/m^2 with flow velocity, u, of 13.71 m/s as shown in Figs. 8, 9 and 10. The thickness of the local conductive sub-layer does not depend on the surface heat flux and the heater inner surface temperature, and that is a constant value 6.52 μm in the wide *z* region. To calculate the nondimensional thickness of the local conductive sublayer, y^+_{CSL}, all properties in the equation are evaluated at the calculated temperature of the first control volume on the heated surface, *TEM*. The dimensionless thickness of the local conduction sublayer for steady-state turbulent heat transfer, y^+_{CSL}, is defined as:

$$y^+_{CSL} = \left(\frac{f_F}{2} \right)^{0.5} \frac{\rho_l u \delta_{CSL}}{\mu_l} \tag{41}$$

where f_F is Fanning friction factor [25-27] and all properties in the equation are evaluated at the average bulk liquid temperature, T_L, [=(T_{in}+(T_{out})$_{cal}$)/2]. The thicknesses and nondimensional thicknesses of local conductive sub-layer, δ_{CSL} and y^+_{CSL}, at various *z* are shown as a red solid line and a pink solid one in Fig. 8 with q=3.009 MW/m^2, Fig. 9 with q=5.176 MW/m^2, and Fig. 10 with q=8.906 MW/m^2 and are listed in

Table 2, 3 and 4, respectively. The thickness of the local conductive sublayer is a constant value 6.52 μm, but the nondimensional thicknesses of the local conductive sublayer (y^+_{CSL}-pink solid line) are 8.224 to 10.297, 8.385 to 12.022, and 8.657 to 15.203 for each heat flux, and become larger with an increase in the *z*-axis distance from the leading edge of the heated section. Its tendency to become higher is almost the same as that of *TEM*.

The numerical solutions of average liquid temperature, $T_{f,av}$, from inlet to outlet are also shown as green broken line in Figs. 8, 9 and 10 for comparison. The average liquid temperatures, $T_{f,av}$, were calculated from the analyzed liquid temperatures of the control volumes on the *r* and θ-axis grid numbers of the *r*-θ plane for each *z*-axis grid number. These increase linearly with increasing z-axis distance, *z*, and are approximately equal to the outlet liquid temperature, T_{out}, at the heated length outlet. Therefore, it was confirmed from this fact that the local liquid temperature experimental results, T_f, obtained by the use of linear interpretation between the inlet and outlet liquid temperatures, T_{in} and T_{out}, would be correct, but these inlet and outlet liquid temperatures were measured with a 1 mm outer diameter sheathed K-type thermocouple in small-diameter tube with d = 3 mm, respectively.

4.2.3. Thickness and nondimensional thickness of local viscous sub-layer, δ_{VSL} and y^+_{VSL}, on forced convection

The Prandtl numbers, $(Pr)_{TEM}$, evaluated at the calculated temperature of the first control volume on the heated surface, *TEM*, and thicknesses and nondimensional thicknesses of local viscous sub-layer at various *z* are shown as a blue solid line, a red 1-dot dashed line and a pink 1-dot dashed line in Figs. 8, 9 and 10 with q=3.009, 5.176 and 8.906 MW/m^2, respectively, and are also listed in Tables 2, 3 and 4. Results of scale analysis in laminar thermal boundary layers give the order of magnitude of the main values shown in following equations [28, 29]:

$$\delta_{VSL} / \delta_{CSL} = (Pr)_{TEM}^{1/2} \quad \text{for } (Pr)_{TEM} << 1 \tag{42}$$

$$y^+_{VSL} / y^+_{CSL} = (Pr)_{TEM}^{1/2} \quad \text{for } (Pr)_{TEM} << 1 \tag{43}$$

$$\delta_{VSL}/\delta_{CSL} = 1 \qquad \text{for } (Pr)_{TEM} = 1 \qquad (44)$$

$$y^+_{VSL}/y^+_{CSL} = 1 \qquad \text{for } (Pr)_{TEM} = 1 \qquad (45)$$

$$\delta_{VSL}/\delta_{CSL} = (Pr)^{1/3}_{TEM} \qquad \text{for } (Pr)_{TEM} > 1 \qquad (46)$$

$$y^+_{VSL}/y^+_{CSL} = (Pr)^{1/3}_{TEM} \qquad \text{for } (Pr)_{TEM} > 1 \qquad (47)$$

The calculated temperatures of the first control volume on the heated surface, *TEM*, become higher as *z* becomes larger, but the Prandtl numbers evaluated at *TEM*, $(Pr)_{TEM}$, decrease gradually with an increase in *z* and those become smaller as the heat flux becomes larger. The thickness of the local conductive sub-layer, δ_{CSL}, did not depend on the surface heat flux and the heater inner surface temperature, and that was a constant value 6.52 μm in the wide *z* region. The thickness and nondimensional thickness of the local viscous sub-layer, δ_{VSL} and y^+_{VSL}, for the turbulent heat transfer on the test tube of d=3 mm and L=33 mm are estimated from Eqs. (42) to (47) with the thickness and nondimensional thickness of the local conductive sub-layer and Prandtl number evaluated at *TEM*. These thicknesses and nondimensional thicknesses of the local viscous sub-layer, δ_{VSL} and y^+_{VSL}, are 10.801 to 9.822 μm and 13.624 to 15.512, 10.703 to 9.237 μm and 13.764 to 17.031, and 10.543 to 8.533 μm and 13.999 to 19.898 in the wide range of the heater inner surface temperature, T_s, at q=3.009, 5.176 and 8.906 MW/m^2, respectively. The thicknesses of the local viscous sub-layer decrease with an increase in the *z*-axis distance from the leading edge of the heated section with a decreasing trend similar to Prandtl number, $(Pr)_{TEM}$, but the nondimensional thicknesses of the local viscous sub-layer increase contrary to that tendency.

And the average values of the thicknesses and nondimensional thicknesses of the local viscous sub-layer, δ_{VSL} and y^+_{VSL}, become 10.054 μm and 15.022, 9.564 μm and 16.156, and 8.938 μm and 18.207 at q=3.009, 5.176 and 8.906 MW/m^2 as shown by the red and pink solid inverted triangle symbols at z=16.5 mm in Figs. 8, 9 and 10, respectively, while those of the thicknesses and nondimensional thicknesses of the local conductive sub-layer, δ_{CSL} and y^+_{CSL}, become 6.52 μm and 9.750, 6.52 μm and 11.038, and 6.52 μm and 13.345 as shown by the red and pink solid triangle symbols. It has been confirmed from these facts that the thickness of the local conductive sub-layer, δ_{CSL}, is constant even over a wide range of heat flux and inner

surface temperature of the test tube and is determined only by the flow velocity while the nondimensional thickness of the local conductive sub-layer, y^+_{CSL}, and, the thickness and nondimensional thickness of the local viscous sub-layer, δ_{VSL} and y^+_{VSL}, vary greatly depending on the heat flux and the inner surface temperature. The thickness of the average conductive sub-layer, $\delta_{CSL,av}$, will be always the same as the thickness of the local conductive sub-layer regardless of the heat flux and the inner surface temperature, and it depends only on the flow velocity as well as the thickness of the local conductive sub-layer, δ_{CSL}.

4.2.4. Thickness and nondimensional thickness of average conductive sub-layer, $\delta_{CSL,av}$ and $y^+_{CSL,av}$, on forced convection

The numerical solutions of the theoretical equations for k-ε turbulence model with high Reynolds number form are in good agreement with the experimental data and the values derived from Eq. (38) within -15 % differences as shown in Fig 7. The thicknesses of the average conductive sub-layer, $\delta_{CSL,av}$, for the turbulent heat transfer on the Pt test tube of d=3 mm and L=32.7 mm in Fig 7 are 17.1, 10.59, 8.24, 6.52, 5.24 and 3.48 μm at flow velocities, u, of 4.222, 7.314, 10.407, 13.715, 17.340 and 21.446 m/s, respectively. These thicknesses of the average conductive sub-layer do not depend on the heat flux and the heater inner surface temperature, and are constant values 17.1, 10.59, 8.24, 6.52, 5.24 and 3.48 μm in the wide ΔT_{sat} region. The heat transfer coefficient, h, is proportional to the reciprocal of the thickness of the conductive sub-layer, $1/\delta_{CSL,av}$ [26]. Mention of the relationship between the heat transfer coefficient, h, and the thickness of the average conductive sub-layer, $\delta_{CSL,av}$, on forced convection in detail are made in Appendix A.1. Relationships between $\delta_{CSL,av}$ and the nondimensional thickness of average conductive sublayer, $y^+_{CSL,av}$, (ΔT_L=100 K) numerically solved for steady-state turbulent heat transfer, and u for d=3 mm, L=33, 67, and 100 mm, and L/d=11, 22.33, and 33.33 with T_{in} of approximately 308 K are shown in Fig. 11 and listed in Table 5. To calculate the nondimensional thicknesses of the average conductive sublayer, $y^+_{CSL,av}$, all properties in the equation are evaluated at the average calculated temperature of the first control volume on the heated surface, TEM_{av}. The nondimensional thicknesses of the average conductive sublayer for steady-state turbulent heat transfer, $y^+_{CSL,av}$, are defined as follows:

$$y^{+}_{CSL,av} = \left(\frac{f_F}{2}\right)^{0.5} \frac{\rho_l u \delta_{CSL,av}}{\mu_l} \tag{48}$$

$$f_F = 0.126\, Re_d^{-0.25} \tag{49}$$

where f_F is Fanning friction factor [25-27] and all properties in the equation are evaluated at the average bulk liquid temperature, T_L, [=(T_{in}+(T_{out})$_{cal}$)/2]. The $\delta_{CSL,av}$ for d = 3 mm with L/d = 11, 22.33, and 33.33 decreased linearly with an increase in flow velocity, u, on a *log–log* scale; however, $y^{+}_{CSL,av}$ increased a little with increase in u but was nevertheless nearly constant over the entire numerical range. These numerical solutions of $\delta_{CSL,av}$ and $y^{+}_{CSL,av}$ (ΔT_L=100 K) for steady-state turbulent heat transfer can be expressed by the following equation determined by the least squares method of power-law:

$$\delta_{CSL,av} = 68.012 u^{-0.9345} \tag{50}$$

$$y^{+}_{CSL,av} = 10.817 u^{0.05563} \qquad \text{for } \Delta T_L = 100 \text{ K} \tag{51}$$

4.2.5. Thickness and nondimensional thickness of average viscous sub-layer, $\delta_{VSL,av}$ and $y^{+}_{VSL,av}$, on forced convection

4.2.5.1. In case of u=4.22 m/s

The typical example of the steady-state turbulent heat transfer curve for Platinum circular tube, d, of 3 mm, heated length, L, of 32.7 mm and heated length-to-inner diameter ratio, L/d, of 10.9 with the exponential period, τ, of around 23.52 s at the flow velocity, u, of 4.22 m/s is re-plotted versus the temperature difference between average inner surface temperature and liquid bulk mean temperature, ΔT_L (=$T_{s,av}$-T_L), as black solid line in Fig. 12. Numerical solution of the relationship between the heat flux, q, and the temperature difference between the average inner surface temperature and the liquid bulk average temperature, ΔT_L, are shown at the flow velocity of 4.22 m/s as green solid circles. The thicknesses of the average conductive sub-layer, $\delta_{CSL,av}$, for the turbulent heat transfer on the Pt test tube of d=3 mm and L=32.7 mm in Fig. 12 is almost constant at 17.1 μm in the wide range of ΔT_L at flow velocity, u, of 4.22 m/s. The Prandtl numbers of the first control volume on the heated surface of the Platinum circular tube on forced convection, $(Pr)_{TEM,av}$, are evaluated at the average calculated temperature of the first control volume on the heated surface, TEM_{av}, and

those are indicated by a blue solid line in Fig. 12. As shown in Fig. 13, the Prandtl numbers of water are given by the following equation with respect to the water temperature.

$$Pr=3.731204E\text{-}13\times *T^{6}\text{-}1.046738E\text{-}9\times T^{5}+1.213098E\text{-}6\times T^{4}\text{-}7.434970E\text{-}4\times T^{3}+ 2.542630E\text{-}1\times T^{2}\text{-}4.604004E1\times T+3.454213E3 \quad (52)$$

The Prandtl number is 4.31 at ΔT_L=8.88 K in Fig. 12. It decreases gradually with an increase in ΔT_L and becomes the value 2.72 at ΔT_L =100.97 K. Further, even when ΔT_L reaches 100.97 K or more, it decreases to minimum value 1.73 at ΔT_L =263.55 K. The thicknesses of average conductive sub-layer, $\delta_{CSL,av}$, are also shown as red solid line in Fig. 12. The thickness of the average conductive sub-layer, $\delta_{CSL,av}$, does not depend on the heat flux and the heater inner surface temperature, and it is a constant value 17.1 μm in the wide ΔT_L region. Results of scale analysis in laminar thermal boundary layers give the order of magnitude of the main values shown in following equations [28, 29]:

$$\delta_{VSL,av}/\delta_{CSL,av}=(Pr)_{TEM,av}^{1/2} \quad \text{for } (Pr)_{TEM,av}<<1 \quad (53)$$

$$\delta_{VSL,av}/\delta_{CSL,av}=1 \quad \text{for } (Pr)_{TEM,av}=1 \quad (54)$$

$$\delta_{VSL,av}/\delta_{CSL,av}=(Pr)_{TEM,av}^{1/3} \quad \text{for } (Pr)_{TEM,av}>1 \quad (55)$$

The thicknesses of the average viscous sub-layer, $\delta_{VSL,av}$, for the turbulent heat transfer on the Pt test tube of d=3 mm and L=32.7 mm at flow velocity, u, of 4.22 m/s are estimated from the thicknesses of the average conductive sub-layer and Prandtl numbers evaluated at the average calculated temperature of the first control volume on the heated surface and those are shown with a red broken line in Fig. 12, and are also listed in Table 6. The thickness of the average viscous sub-layer, $\delta_{VSL,av}$, is 27.825 μm at ΔT_L=8.88 K. It decreases gradually with decreasing trend similar to Prandtl number, $(Pr)_{TEM,av}$, as ΔT_L increases and becomes the value 23.859 μm at ΔT_L =100.97 K. Further, when ΔT_L is 100.97 K or more, it decreases also to minimum value 20.525 μm at ΔT_L =263.55 K. The nondimensional thicknesses of average conductive sub-layer, $y^+_{CSL,av}$, are also shown as pink solid line in Fig. 12 and are listed in Table 6. As described above, the thickness of the average conductive sub-layer is a constant value 17.1 μm in the wide ΔT_L region, but the nondimensional thickness of the average conductive sub-layer, $y^+_{CSL,av}$, becomes higher with an increase in ΔT_L due to the temperature dependence of the thermo-physical property value. The nondimensional thicknesses of the

average viscous sub-layer, $y^+_{VSL,av}$, are calculated by the following equations and are indicated by a pink broken line in the figure and are listed in the table.

$$y^+_{VSL,av} \Big/ y^+_{CSL,av} = (Pr)^{1/2}_{TEM,av} \quad \text{for } (Pr)_{TEM,av} \ll 1 \tag{56}$$

$$y^+_{VSL,av} \Big/ y^+_{CSL,av} = 1 \quad \text{for } (Pr)_{TEM,av} = 1 \tag{57}$$

$$y^+_{VSL,av} \Big/ y^+_{CSL,av} = (Pr)^{1/3}_{TEM,av} \quad \text{for } (Pr)_{TEM,av} > 1 \tag{58}$$

The nondimensional thickness of the average viscous sub-layer, $y^+_{VSL,av}$, is similar to the temperature rise tendency of the nondimension thickness of the average conductive sub-layer, $y^+_{CSL,av}$, and it increases as the ΔT_L increases.

The thickness of the local conductive sub-layer, δ_{CSL}, for the turbulent heat transfer on the Pt test tube of d=3 mm and L=32.7 mm is constant at 17.1 μm in the wide range of heater inner surface temperature, T_s, at flow velocity, u, of 4.22 m/s. The thickness of the local conductive sub-layer, δ_{CSL}, does not also depend on the heat flux and the heater inner surface temperature, and is a constant value 17.1 μm in the wide ΔT_L region. For this reason, the thickness of the average conductive sub-layer, $\delta_{CSL,av}$, is exactly the same value as the thickness of the local conductive sub-layer, δ_{CSL}. The nondimensional thickness of the local conductive sub-layer, y^+_{CSL}, and, the thickness and nondimensional thickness of the local viscous sub-layer, δ_{VSL} and y^+_{VSL}, for the turbulent heat transfer are estimated from the thickness of the local conductive sub-layer, δ_{CSL}, and Prandtl numbers evaluated at the calculated temperature of the first control volume on the heated surface, $(Pr)_{TEM}$. Mentions of the thickness and nondimensional thickness of local conductive sub-layer, δ_{CSL} and y^+_{CSL}, and the thickness and nondimensional thickness of local viscous sub-layer, δ_{VSL} and y^+_{VSL}, on forced convection in detail are made in **4.2.2** and **4.2.3**.

4.2.5.2. In cases of u=7.31, 10.41, 13.72, 17.34 and 21.45 m/s

Heat transfer processes on the Pt test tube of d=3 mm and L=32.7 mm compared with heat transfer curves

numerically analyzed, Prandtl numbers evaluated at the average calculated temperature of the first control volume on the heated surface under forced convection, thicknesses of conductive and viscous sub-layers and nondimensional thicknesses of conductive and viscous sub-layers at various ΔT_L are shown in Fig. 14 and Table 7 with u=7.31 m/s, Fig. 15 and Table 8 with u=10.41 m/s, Fig. 16 and Table 9 with u=13.72 m/s, Fig. 17 and Table 10 with u=17.34 m/s, and Fig. 18 and Table 11 with u=21.45 m/s, respectively. The Prandtl numbers evaluated at the average calculated temperature of the first control volume on the heated surface of the Platinum circular tube on forced convection, $(Pr)_{TEM,av}$, decrease gradually with an increase in ΔT_L and becomes finally the minimum at the maximum value of ΔT_L. The thicknesses of the average conductive sub-layer, δ_{CSLav}, do not depend on the heat flux and the heater inner surface temperature, and are constant values 10.59, 8.24, 6.52, 5.24 and 3.48 μm in the wide ΔT_L region at each fixed flow velocity. The thicknesses of the average viscous sub-layer, $\delta_{VSL,av}$, for the turbulent heat transfer on the Pt test tube of d=3 mm and L=32.7 mm are estimated from the thicknesses of the average conductive sub-layer and Prandtl numbers evaluated at the average calculated temperature of the first control volume on the heated surface, and those are shown with a red broken line in Figs. 14, 15, 16, 17 and 18, and are also listed in Tables 7 to 11. These thicknesses of the average viscous sub-layer, $\delta_{VSL,av}$, are 17.497 to 13.719 μm, 13.618 to 9.969 μm, 10.743 to 7.992 μm, 8.572 to 6.604 μm, and 5.499 to 3.880 μm in the wide range of ΔT_L at u=7.31, 10.41, 13.72, 17.34 and 21.45 m/s, respectively. Those decrease gradually with decreasing trend similar to Prandtl number, $(Pr)_{TEM,av}$, as ΔT_L increases and become the minimum values 13.72, 9.97, 7.99, 6.60 and 3.88 μm at ΔT_L =161.02, 236.66, 216.89, 169.63 and 249.96 K. The nondimensional thicknesses of average conductive and viscous sub-layers, $y^+_{CSL,av}$ and $y^+_{VSL,av}$, are also shown as pink solid and broken lines in Figs. 14 to 18. As described above, the thicknesses of the average conductive sub-layer are constant values 10.59, 8.24, 6.52, 5.24 and 3.48 μm in the wide ΔT_L region, respectively, but the nondimensional thicknesses of the average conductive sub-layer become higher with an increase in ΔT_L due to the temperature dependence of the thermo-physical property value. The nondimensional thicknesses of the average viscous sub-layer, $y^+_{VSL,av}$, are similar to the temperature rise tendency of the nondimension thicknesses of the average conductive sub-layer, $y^+_{CSL,av}$, and those increase as the ΔT_L increases.

4.2.5.3. Influence of heated length on $\delta_{CSL,av}$, $y^+_{CSL,av}$, $\delta_{VSL,av}$ and $y^+_{VSL,av}$

Relationships between the thickness and nondimensional thickness of average conductive sub-layer, $\delta_{CSL,av}$ and $y^+_{CSL,av}$, and the heated length, L, numerically solved with d = 3 mm and L = 33, 67, and 100 mm at T_{in} of approximately 306 K are presented in Fig. 19. Both $\delta_{CSL,av}$ and $y^+_{CSL,av}$ are nearly constant for various heated lengths on a semi-log scale. The $y^+_{CSL,av}$ are the values at ΔT_L =100 K.

The $\delta_{VSL,av}$ at ΔT_L=100 K for d = 3 mm with L/d = 11, 22.33, and 33.33 decreased linearly with an increase in flow velocity, u, on a *log–log* scale in Fig. 20; however, $y^+_{VSL,av}$ increased a little with an increase in u but was nevertheless nearly constant over the entire numerical range. These numerical solutions of $\delta_{VSL,av}$ and $y^+_{VSL,av}$ at ΔT_L=100 K for steady-state turbulent heat transfer can be expressed by the following equation determined by the least squares method of power-law:

$$\delta_{VSL,av} = 103.837 u^{-0.9792} \qquad \text{for } \Delta T_L = 100 \text{ K} \tag{59}$$

$$y^+_{VSL,av} = 16.519 u^{0.01088} \qquad \text{for } \Delta T_L = 100 \text{ K} \tag{60}$$

Relationships between the thickness and nondimensional thickness of average viscous sub-layer, $\delta_{VSL,av}$ and $y^+_{VSL,av}$, at ΔT_L=100 K, and the heated length, L, numerically solved with d = 3 mm and L = 33, 67, and 100 mm at T_{in} of approximately 306 K are presented in Fig. 21 and listed in Table 12. Both $\delta_{VSL,av}$ and $y^+_{VSL,av}$ are nearly constant for various heated lengths on a semi-log scale. The $\delta_{VSL,av}$ and $y^+_{VSL,av}$ are the values at ΔT_L =100 K.

4.2.6. Thickness of conductive sub-layer on nucleate boiling heat transfer, δ

The heat transfer with thinner conductive sub-layer dissipated by the evaporation on nucleate boiling is numerically analyzed by the theoretical equations for steady-state turbulent heat transfer. Numerical solution of the relationship between the heat flux, q, and the temperature difference between the average inner surface temperature and the liquid bulk average temperature, ΔT_L, are shown for the heat flux, q, ranging from 6.57×10^5 to 1.74×10^7 W/m^2, from 6.54×10^5 to 2.52×10^7 W/m^2, from 6.48×10^5 to 3.42×10^7 W/m^2, from 6.47×10^5 to 4.29×10^7 W/m^2, from 1.29×10^6 to 4.93×10^7 W/m^2 and from 1.88×10^6 to 3.84×10^7 W/m^2 at the

flow velocities of 4.222, 7.314, 10.407, 13.715, 17.340 and 21.446 m/s as colored solid circles in Figs. 22 to 27, respectively. The 12-13, 12-14, 14, 12-14, 14 and 14 different values for the numerical solutions are plotted for the ΔT_L ranging from 5.76 to 348.97 K, from 5.45 to 266.36 K, from 5.60 to 293.26 K, from 5.51 to 262.65 K, from 7.14 to 288.87 K and from 6.61 to 180.27 K on the *log q* versus *log* ΔT_L graph, respectively. These solutions for δ=6.43, 1.73 and 0.33 μm, δ=5.24, 1.97, 0.57 and 0.11 μm, δ=4.25, 1.64, 0.48 and 0.09 μm, δ=3.48, 1.37, 0.41 and 0.13 μm, δ=2.86, 1.15 and 0.48 μm and δ=1.97, 0.81 and 0.25 μm become also higher with an increase in the ΔT_L on the higher curves parallel to the steady-state turbulent heat transfer one derived from Eq. (38) as shown in Figs. 22 to 27, respectively. The outer control volume widths for the *r*-component, $(\Delta r)_{out}$, which are twice as large as the thicknesses of the conductive sub-layer, δ, are ranging from 12.86 to 0.66 μm, ranging from 10.48 to 0.22 μm, ranging from 8.5 to 0.18 μm, ranging from 6.96 to 0.26 μm, ranging from 5.72 to 0.96 μm and ranging from 3.94 to 0.5 μm at flow velocities, *u*, of 4.222, 7.314, 10.407, 13.715, 17.340 and 21.446 m/s, respectively. These curve-fitted numerical solutions based on the least squares method of power-law are shown in Figs. 22 to 27. The thicknesses of the conductive sub-layer, δ, on the nucleate boiling heat transfer experimentally obtained would become half the outer control volume width for the *r*-component, $(\Delta r)_{out}/2$, numerically solved at an intersection point between the fully-developed nucleate boiling heat transfer curves and the smoothing curves of conductive sub-layer.

It has been assumed that the measurement of thickness of the conductive sub-layer at CHF point would be very useful to discuss the mechanism of the critical heat flux during flow boiling of subcooled water, which would occur due to the heterogeneous spontaneous nucleation at the lower limit of the heterogeneous spontaneous nucleation temperature [12], due to hydrodynamic instability suggested by Kutateladze [13] and Zuber [14] or due to the liquid sub-layer dry-out models suggested by Lee and Mudawar [15], Katto [16] and Celata et. al. [17]. The thicknesses of the average conductive sub-layer on forced convection and nucleate boiling heat transfer, $\delta_{CSL,av}$ and δ, are shown versus heat flux, *q*, for the *u* ranging from 4 to 21 m/s in Fig. 28. These thicknesses on the semi-log graph ($\delta_{CSL,av}$ and δ versus *log q*) become linearly lower with an increase in the *q*. Those look like being almost 0 μm at the CHF points, although that at *u*=4 m/s becomes almost 0 μm at the heat flux 30.77 % lower than the CHF one. The conductive sub-layer at CHF point would

have almost disappeared, however, an intense boiling sound occurred for a period of time before the CHF point. As shown in Fig. 29, the ratios of conductive sub-layer on nucleate boiling heat transfer to conductive sub-layer on forced convection, $\delta_{CSL,av}/\delta_{CSL,av}$ and $\delta/\delta_{CSL,av}$, for the Pt test tube of d=3 mm and L=32.7 mm with the commercial finish of inner surface can be expressed for the ratios of boiling number on nucleate boiling heat transfer to boiling number at CHF point, Bo/Bo_{cr}, for the u ranging from 4 to 21 m/s by the following correlations:

$$\frac{\delta}{\delta_{CSL,av}} = -0.79989 ln\left(\frac{1}{0.84419}\frac{Bo}{Bo_{cr}}\right) \quad \text{for } u\text{=4 m/s} \tag{61}$$

$$\frac{\delta}{\delta_{CSL,av}} = -0.84353 ln\left(\frac{1}{0.82275}\frac{Bo}{Bo_{cr}}\right) \quad \text{for } u\text{=6.9 m/s} \tag{62}$$

$$\frac{\delta}{\delta_{CSL,av}} = -0.88649 ln\left(\frac{1}{0.90454}\frac{Bo}{Bo_{cr}}\right) \quad \text{for } u\text{=9.9 m/s} \tag{63}$$

$$\frac{\delta}{\delta_{CSL,av}} = -0.88072 ln\left(\frac{1}{0.92842}\frac{Bo}{Bo_{cr}}\right) \quad \text{for } u\text{=13.3 m/s} \tag{64}$$

$$\frac{\delta}{\delta_{CSL,av}} = -0.87898 ln\left(\frac{1}{1.00626}\frac{Bo}{Bo_{cr}}\right) \quad \text{for } u\text{=17 m/s} \tag{65}$$

$$\frac{\delta}{\delta_{CSL,av}} = -1.14810 ln\left(\frac{1}{1.08001}\frac{Bo}{Bo_{cr}}\right) \quad \text{for } u\text{=21 m/s} \tag{66}$$

It is assumed that the transition to film boiling at the subcooled water flow boiling on the Pt test tube of d=3 mm and L=32.7 mm would occur due to the **liquid sub-layer dry-out model** [15-17] at the steady-state CHF but not due to the heterogeneous spontaneous nucleation [12] and the hydro-dynamic instability [13, 14]. The conductive sub-layer at CHF point has almost disappeared under the u ranging from 4 to 21 m/s, and it would not be seen that the CHF phenomenon occurs at some critical velocity in the vapor phase when the vapor jets and the liquid ones start interfering with each other. It is the reason not to occur the hydrodynamic instability on the vapor-liquid interface at the CHF.

The values of CHF numerically analyzed from Celata et. al.'s liquid sub-layer dry-out model [17] are shown in Figs. 22 to 29 for comparison. The values derived from liquid sub-layer dry-out model are in good agreement with the experimental values of CHF for the Pt test tube of d=3 mm and L=32.7 mm within -21.10 to 0.49 % differences at whole u range of 4.222, 7.314, 10.407, 13.715, 17.340 and 21.446 m/s tested here

and the values of heat flux at which the thicknesses of the conductive sub-layer become 0 μ-m. The relationship between $\delta_{CSL}/\delta_{CSL}$ and δ/δ_{CSL}, and Bo/Bo_{cr} at a flow velocity from 4 to 21 m/s is almost represented by one display formula shown below instead of Eqs. (61) to (66) in Fig. 29.

$$\frac{\delta}{\delta_{CSL}} = -0.18013 ln\left(\frac{Re_d}{357.24}\right) ln\left\{\frac{\frac{Bo}{Bo_{cr}}}{0.21656 ln\left(\frac{Re_d}{927.94}\right)}\right\} \tag{67}$$

4.3. Comparison of the Measured CHFs with Author's Correlations, and Other Researchers' CHF Model and Correlations

Figure 30 shows the steady-state CHF, $q_{cr,sub,st}$, outlet subcooling, $T_{sub,out}$, of a vertical Pt circular test tube with an inner diameter (d = 3 mm) and a heated length (L = 32.7 mm), L / d (= 10.9) and wall thickness (δ = 0.5 mm) are obtained at flow velocities u ranging from 4 to 21 m / s at an outlet pressure, P_{out}, of about 800 kPa. As shown in the figure, $q_{cr,sub,st}$ for each flow velocity increase with increasing $\Delta T_{sub,out}$ and the rate of increase decreases with increasing $\Delta T_{sub,out}$. CHF throughout the experimental range increases with increasing flow rate at fixed $\Delta T_{sub,out}$. The curves given by Eqs. (68) and (69) for a vertical SUS304 circular test tube are shown in Fig. 30 at each flow velocity for comparison.

Outlet subcooling:

$$Bo_{cr} = 0.082 D^{*-0.1} We^{-0.3} \left(\frac{L}{d}\right)^{-0.1} Sc^{0.7} \qquad \text{for } \Delta T_{sub,out} \geq 30 \text{ K and } u \leq 13.3 \text{ m/s [1, 4]} \tag{68}$$

$$Bo_{cr} = 0.0418 D^{*-0.175} We^{-0.225} \left(\frac{L}{d}\right)^{-0.1} Sc^{0.7} \qquad \text{for } \Delta T_{sub,out} \geq 30 \text{ K and } u > 13.3 \text{ m/s [6]} \tag{69}$$

Inlet subcooling:

$$Bo_{cr} = C_1 D^{*-0.1} We^{-0.3} \left(\frac{L}{d}\right)^{-0.1} e^{-\frac{(L/d)}{C_2 Re_d^{0.4}}} Sc^{*C_3} \qquad \text{for } \Delta T_{sub,in} \geq 40 \text{ K and } u \leq 13.3 \text{ m/s[2, 3, 4]} \tag{70}$$

$$Bo_{cr} = C_4 D^{*-0.175} We^{-0.225} \left(\frac{L}{d}\right)^{-0.1} e^{-\frac{(L/d)}{C_5 Re_d^{0.5}}} Sc^{*C_6} \qquad \text{for } \Delta T_{sub,in} \geq 40 \text{ K and } u > 13.3 \text{ m/s [6]} \tag{71}$$

where C_1=0.082, C_2=0.53 and C_3=0.7 for L/d≤around 40 [2] and C_1=0.092, C_2=0.85 and C_3=0.9 for L/d>around 40 [3]. C_4=0.0418, C_5=0.144 and C_6=0.7 for L/d≤around 40 [6] and C_4=0.0469, C_5=0.231 and C_6=0.9 for L/d>around 40 [6]. Bo_{cr}, D^*, We, Sc and Sc^* are boiling number ($=q_{cr,sub}/Gh_{fg}$), non-dimensional diameter [$D^*=d/\{\sigma/g/(\rho_l-\rho_g)\}^{0.5}$], Weber number ($=G^2d/\rho_l\sigma$), non-dimensional outlet subcooling ($=c_{pl}\Delta T_{sub,out}/h_{fg}$) and non-dimensional inlet subcooling ($Sc^*=c_{pl}\Delta T_{sub,in}/h_{fg}$), respectively [1-6]. CHF data for $\Delta T_{sub,out}\geq$ 30 K agree well with the values given by correlations. Equations (68) and (69) were derived based on the experimental data for the vertical SUS304 test tube with the flow velocities ranging from 4 to 13.3 m/s [1-4] and ranging from 17 to 40 m/s [6] respectively. To confirm the applicability of Eqs. (68) and (69) to data at flow velocities of 4-21 m/s, the ratio of these CHF data to the corresponding values calculated by Eqs. (68) and (69) is shown for $\Delta T_{sub,out}$ in Fig. 31. Most data for vertical circular test tubes (14 points) are within -22.74 to -6.04 % differences for 4.10 m/s≤u≤21.21 m/s and 94.34 K≤$\Delta T_{sub,out}$≤116.29 K.

It can be considered that the CHFs are determined not by the outlet conditions but by the inlet ones. Steady-state CHF, $q_{cr,sub,st}$, of a vertical Pt circular test tube with an inner diameter of 3 mm, L= 32.7 mm, L/d = 10.9 and δ = 0.5 mm was shown for the inlet subcooling, $\Delta T_{sub,in}$, at a flow velocities of 4-21 m/s in Fig. 32. The $q_{cr,sub,st}$ for each flow velocity increases with increasing $\Delta T_{sub,in}$. The higher the $\Delta T_{sub,in}$, the lower the rate of increase. The $q_{cr,sub,st}$ increases with increasing flow velocity with fixed $\Delta T_{sub,in}$. The $q_{cr,sub,st}$ for a wide range of flow velocities are proportional to $\Delta T_{sub,in}^{0.7}$ for $\Delta T_{sub,in}\geq$ 40 K. The curves obtained from Eqs. (70) and (71) for a vertical SUS304 circular test tube are shown in Fig. 32 for comparison. CHF data for $\Delta T_{sub,in}\geq$ 40 K are in good agreement with values given by author correlations. To confirm the applicability of Eqs. (70) and (71), the ratio of the CHF data for these d = 3 mm vertical circular test tubes (14 points) to the corresponding values calculated in Eqs. (70) and (71) is shown for $\Delta T_{sub,in}$ in Fig. 33. Most data of $\Delta T_{sub,in}\geq$ 40 K are within -19.81 to -6.21 % differences of Eqs. (70) and (71) for 4.10 m/s≤u≤21.21 m/s and 134.70 K≤$\Delta T_{sub,in}$≤139.14 K.

Celata et al. [17] presented a mechanistic model for prediction of CHF in flow boiling of subcooled water. Hall and Mudawar [33] developed the inlet and outlet condition correlations for subcooled high-CHF based

on the experimental data. Hall and Mudawar correlation [33] for the outlet conditions is as follows:

$$Bo_{cr} = 0.0332We^{-0.235}\left(\frac{\rho_l}{\rho_g}\right)^{-0.681}\left[1-0.6837\left(\frac{\rho_l}{\rho_g}\right)^{0.832}\chi_{out}\right] \quad \text{for outlet} \tag{72}$$

Shah [34, 35] presented the upstream-conditions correlation (UCC) and the local-conditions correlation (LCC) for CHF in vertical tubes. Shah correlation for the LCC version [35] is as follows:

$$Bo_{cr} = F_E F_x Bo_0 \quad \text{for the LCC version} \tag{73}$$

The experimental data for u=4 to 21 m/s at P_{out}=800 kPa are compare with authors' correlations, Eqs. (68) and (69), solutions of the model by Celata et al. [17], Hall and Mudawar correlation, Eq. (72), [33] and Shah correlation for the LCC version, Eq. (73), [34, 35] in Fig. 34 for the THD-F173 Pt test tube of d=3 mm and L=32.7 mm with the commercial finish of inner surface. The authors' correlations, Eqs. (68) and (69), solutions of the model by Celata et al., Hall and Mudawar correlation, Eq. (72), and Shah correlation for the LCC version, Eq. (73), are in good agreement with the experimental data for u=4 to 21 m/s within -22.74 to -6.04 % differences, -21.10 to 0.49 % differences, -22.17 to 0.58 % differences and -19.20 to 6.16 % differences, respectively.

5. CONCLUSIONS

Subcooled boiling heat transfer and steady state critical heat flux (CHF) in a vertical tube for the liquid Reynolds numbers (Re_d=2.35×10^4 to 1.12×10^5) and the flow velocities (u=4.103 to 21.446 m/s) at the inlet liquid temperatures (T_{in}=308.20 to 311.28 K) and the inlet pressures (P_{in}=831.51 to 942.94 kPa) are systematically measured. Pt tube with inner diameter d = 3mm, heated length L = 32.7mm and L / d = 10.9 is used. On the other hand, the RANS equations with k-ε turbulence model are numerically solved with various thicknesses of conductive sub-layer. Experimental and computational study results lead as follows:

1) The thickness of the local conductive sub-layer, δ_{CSL}, does not depend on the heat flux and the heater inner surface temperature, and is a constant value in the wide ΔT_L region. Therefore, the thickness of the average conductive sub-layer, $\delta_{CSL,av}$, is exactly the same value as the thickness of the local conductive sub-layer, δ_{CSL}.

2) The thicknesses of the average conductive sub-layer, $\delta_{CSL,av}$, for the turbulent heat transfer are 17.1, 10.59, 8.24, 6.52, 5.24 and 3.48 μm at flow velocities, u, of 4.222, 7.314, 10.407, 13.715, 17.340 and 21.446 m/s, respectively.

3) The thickness of the average conductive sub-layer, $\delta_{CSL,av}$, does not depend on the heat flux and the heater inner surface temperature, and it is a constant value in the wide ΔT_L region, but the nondimensional thickness of the average conductive sub-layer, $y^+_{CSL,av}$, becomes higher with an increase in ΔT_L due to the temperature dependence of the thermo-physical property value.

4) The thicknesses of the average viscous sub-layer, $\delta_{VSL,av}$, on forced convection are estimated from the thicknesses of the average conductive sub-layer and Prandtl numbers evaluated at the average calculated temperature of the first control volume on the heated surface. These thicknesses of the average viscous sub-layer, δ_{VSL}, are 27.825 to 20.525 μm, 17.497 to 13.719 μm, 13.618 to 9.969 μm, 10.743 to 7.992 μm, 8.572 to 6.604 μm, and 5.499 to 3.880 μm in the wide range of ΔT_L at u=4.22, 7.31, 10.41, 13.72, 17.34 and 21.45 m/s, respectively. The nondimensional thicknesses of the average viscous sub-layer, $y^+_{VSL,av}$, are similar to the temperature rise tendency of the nondimension thicknesses of the average conductive sub-layer, $y^+_{CSL,av}$, and those increase as the ΔT_L increases.

5) The relationship between $\delta_{CSL,av}/\delta_{CSL,av}$ and $\delta/\delta_{CSL,av}$, and Bo/Bo_{cr} at a flow velocity from 4 to 21 m/s is almost represented by one display formula shown below:

$$\frac{\delta}{\delta_{CSL}} = -0.18013 ln\left(\frac{Re_d}{357.24}\right) ln\left\{\frac{\frac{Bo}{Bo_{cr}}}{0.21656 ln\left(\frac{Re_d}{927.94}\right)}\right\} \tag{67}$$

6) The transition to film boiling at the subcooled water flow boiling on the Pt test tube of d=3 mm and L=32.7 mm would occur due to the **liquid sub-layer dry-out model** [15-17] at the steady-state CHF.

7) Most of the steady-state CHF data at high liquid Reynolds number with 4.10 m/s≤u≤21.21 m/s (14 points) are within -22.74 to -6.04 % differences of Eqs. (68) and (69) for 94.34 K≤$\Delta T_{sub,out}$≤116.29 K and within -19.81 to -6.21 % differences of Eqs. (70) and (71) for 4.10 m/s≤u≤21.21 m/s and 134.70 K≤$\Delta T_{sub,in}$≤1392.14 K.

8) The solutions of the model by Celata et al. [17], Hall and Mudawar correlation, Eq. (72), [33] and Shah correlation for the LCC version, Eq. (73), [34, 35] are in good agreement with the experimental data for

u=4 to 21 m/s within -21.10 to 0.49 % differences, -22.17 to 0.58 % differences and -19.20 to 6.16 % differences, respectively.

NOMENCLATURE

Bo $=q/Gh_{fg}$, boiling number

Bo_{cr} $=q_{cr,sub,st}/Gh_{fg}$, boiling number at CHF point

C_1, C_2, C_3, C_4, C_5, C_6 constants in Eqs. (70) and (71)

c_{pl} specific heat at constant pressure, J/kgK

d test tube inner diameter, m

f_F Fanning friction factor

G $=\rho_l u$, mass velocity, kg/m^{2}s

h_{fg} latent heat of vaporization, J/kg

L heated length, m

L_{eff} effective length, m

Nu_d $=hd/\lambda_l$, nusselt number

P_{cr} =22064 kPa, critical pressure, kPa

P_{in} pressure at inlet of heated section, kPa

P_{ipt} pressure measured by inlet pressure transducer, kPa

P_{out} pressure at outlet of heated section, kPa

P_{opt} pressure measured by outlet pressure transducer, kPa

Pr $=c_p\mu/\lambda$, Prandtl number

$(Pr)_{TEM}$ Prandtl number evaluated at the calculated temperature of the first control volume on the heated surface under forced convection

$(Pr)_{TEM,av}$ Prandtl number evaluated at the average calculated temperature of the first control volume on the heated surface under forced convection

Q heat generation rate per unit volume, W/m^3

Q_0 initial exponential heat input, W/m^3

q heat flux, W/m^2

$q_{cr,sub,st}$ steady-state CHF for subcooled condition, W/m^2

Ra average roughness, μm

Re_d $=Gd/\mu_l$, Reynolds number

$Rmax$ maximum roughness depth, μm

Rz mean roughness depth, μm

r_i test tube inner radius, m

r_o test tube outer radius, m

$(\Delta r)_{out}$ outer control volume width for r-component, m

TEM calculated temperature of the first control volume on the heated surface, K

TEM_{av} average calculated temperature of the first control volume on the heated surface, K

T water temperature, C

$\overline{T}$ average temperature of test tube, K

$T_{f,av}$ average liquid temperature, K

T_{in} inlet liquid temperature, K

T_L $=(T_{in}+T_{out})/2$, liquid bulk mean temperature, K

T_{out} outlet liquid temperature, K

T_s heater inner surface temperature, K

T_{sat} saturation temperature, K

T_{so} heater outer surface temperatures, K

$T_{s,av}$ average inner surface temperature, K

ΔT_L $=(T_{s,av}-T_L)$, temperature difference between average inner surface temperature and liquid bulk mean temperature, K

ΔT_{sat} $=T_s-T_{sat}$, inner surface superheat, K

u flow velocity, m/s

y^+ $=y(\tau_w\rho_l)^{0.5}/\nu_l$, dimensionless normal-distance coordinate

y^+_{CSL} $=(f_F/2)^{0.5}\rho_l u \delta_{CSL}/\mu_l$, non-dimensional thickness of local conductive sub-layer

$y^+_{CSL,av}$ $=(f_F/2)^{0.5}\rho_l u \delta_{CSL,av}/\mu_l$, non-dimensional thickness of average conductive sub-layer

y^+_{VSL} $=(f_F/2)^{0.5}\rho_l u \delta_{CSL}/\mu_l$, non-dimensional thickness of local viscous sub-layer

$y^+_{VSL,av}$ $=(f_F/2)^{0.5}\rho_l u \delta_{CSL,av}/\mu_l$, non-dimensional thickness of average viscous sub-layer

z z-axis distance from the leading edge of the heated section, m

δ conductive sub-layer on nucleate boiling heat transfer

δ_{CSL} $=(\Delta r)_{out}/2$, thickness of local conductive sub-layer on forced convection

$\delta_{CSL,av}$ $=(\Delta r)_{out}/2$, thickness of average conductive sub-layer on forced convection

δ_{VSL} thickness of local viscous sub-layer on forced convection

$\delta_{VSL,av}$ thickness of average viscous sub-layer on forced convection

ε rate of dissipation of turbulent energy, m^2/s^3

μ_l viscosity, Ns/m^2

μ_w viscosity at tube wall temperature, Ns/m^2

ν_l $=\mu_l/\rho_l$, kinematic viscosity of fluid, Ns m/kg

ρ_l density of fluid, kg/m^3

τ_w shear stress at the wall, N/m^2

χ vapor quality

ACKNOWLEDGMENTS

This research was performed as a LHD joint research project of NIFS (National Institute for Fusion Science), Japan, NIFS17KEMF100, 2017, 2018 and 2019.

REFERENCES

1. K. Hata, M. Shiotsu and N. Noda, "Critical Heat Fluxes of Subcooled Water Flow Boiling against Outlet Subcooling in Short Vertical Tube," *Journal of Heat Transfer*, Trans. ASME, Series C, **126**, pp. 312-320 (2004).
2. K. Hata, H. Komori, M. Shiotsu and N. Noda, "Critical Heat Fluxes of Subcooled Water Flow Boiling against Inlet Subcooling in Short Vertical Tube," *JSME International Journal*, Series B, **47**(2), pp. 306-315 (2004).
3. K. Hata, M. Shiotsu and N. Noda, "Critical Heat Flux of Subcooled Water Flow Boiling for High L/d Region," *Nuclear Science and Engineering*, **154**(1), pp. 94-109 (2006).
4. K. Hata and S. Masuzaki, "Subcooled Boiling Heat Transfer in a Short Vertical SUS304-Tube at Liquid Reynolds Number Range 5.19×10^4 to 7.43×10^5," *Nuclear Engineering and Design*, **239**, pp. 2885-2907 (2009).
5. K. Hata and S. Masuzaki, "Subcooled Boiling Heat Transfer for Turbulent Flow of Water in a Short Vertical Tube," *Journal of Heat Transfer*, Trans. ASME, Series C, **132**, pp. 011501-1-11 (2010).
6. K. Hata and S. Masuzaki, "Critical Heat Fluxes of Subcooled Water Flow Boiling in a Short Vertical Tube at High Liquid Reynolds Number," *Nuclear Engineering and Design*, **240**, pp. 3145-3157 (2010).
7. K. Hata, Y. Shirai and S. Masuzaki, "Heat Transfer and Critical Heat Flux of Subcooled Water Flow Boiling in a Horizontal Circular Tube," *Experimental Thermal and Fluid Science*, **44**, pp. 844-857 (2013).
8. K. Hata, K. Fukuda and S. Masuzaki, "Transient Critical Heat Fluxes of Subcooled Water Flow Boiling in a SUS304-Circular Tube with Various Twisted-Tape Inserts (Influence of Twist Ratio)," *Journal of Thermal Science and Engineering Applications,* Trans. ASME, **6**, pp. 031010-1-14 (2014).
9. K. Hata, K. Fukuda and S. Masuzaki, "Mechanism of Critical Heat Flux during Flow Boiling of Subcooled Water in a Circular Tube at High Liquid Reynolds Number," *Experimental Thermal and Fluid Science*, http://dx.doi.org/10.1016/j.expthermflusci.2015.09.015, **70**, pp. 255-269 (2016).
10. K. Hata, K. Fukuda and S., Masuzaki, "Influence of Boiling Initiation Surface Superheat on Subcooled Water Flow Boiling Critical Heat Flux in a SUS304 Circular Tube at High Liquid Reynolds Number," *International Journal of Heat and Mass Transfer*, http://dx.doi.org/10.1016/j.ijheatmasstransfer.2016.03.017, **98**, pp. 299-312 (2016).
11. K., Hata, Q.S., Liu, and S., Masuzaki, "Conductive and Viscous Sub-layers on Forced Convection and

Mechanism of Critical Heat Flux during Flow Boiling of Subcooled Water in a Circular Tube at High Liquid Reynolds Number," *Heat and Mass Transfer,* DOI: 10.1007/s00231-018-2458-4, **55**, pp.175-195 (2019).

12. C. Cole, *Homogeneous and heterogeneous nucleation in Boiling Phenomena*, **1**, Stralen, S. van, and Cole, R. eds., Hemisphere Pub. Corp., p. 71, (1979).
13. S.S. Kutateladze, *Heat Transfer in Condensation and Boiling*, AEC-tr-3770, USAEC (1959).
14. N. Zuber, *Hydrodynamic Aspects of Boiling Heat Transfer*, AECU-4439, USAEC (1959).
15. C.H. Lee and I. Mudawar, "A mechanistic critical heat flux model for subcooled flow boiling based on local bulk flow conditions," *International Journal of Multiphase Flow*, **14**, pp. 711-728 (1988).
16. Y., Katto, "A physical approach to critical heat flux of subcooled flow boiling in round tubes," *International Journal of Heat and Mass Transfer*, **33**(4), pp. 611-620 (1990).
17. G. P. Celata, M. Cumo, A. Mariani, M. Simoncini and G. Zummo, "Rationalization of existing mechanistic models for the prediction of water subcooled flow boiling critical heat flux," *International Journal of Heat and Mass Transfer*, **37**, suppl. 1, pp. 347-360 (1994).
18. W.P. Jones and B.E., Launder, "The Prediction of Laminarization with a Two- equation Model of Turbulence," *Int. J. Heat Mass Transfer*, **15**, pp.301–314 (1972).
19. D.B. Spalding, *The PHOENICS Beginner's Guide*, CHAM Ltd., London, United Kingdom (1991).
20. PHOENICS Nihongo Manyuaru (PHOENICS Japanese Manual), CHAM-Japan, Tokyo (in Japanese) (2010).
21. S.V. Patankar, *Numerical Heat Transfer and Fluid Flow*, Hemisphere Pub. Corp., New York (1980).
22. S.V. Patankar, and D.B. Spalding, "A Calculation Procedure for Heat, Mass and Momentum Transfer in Three-Dimensional Parabolic Flows," *Int. J. Heat Mass Transfer*, **15**, pp.1787–1806 (1972).
23. K. Hata, Y. Shirai, S. Masuzaki and A. Hamura, "Computational Study of Turbulent Heat Transfer for Heating of Water in a Short Vertical Tube under Velocities Controlled," *Nuclear Engineering and Design*, **249**, pp. 304-317 (2012).
24. K. Hata, Y. Shirai, S. Masuzaki and A. Hamura, "Computational Study of Turbulent Heat T eating of Water in a Vertical Circular Tube –Influence of Tube Inner Diameter on Thickness of Conductive Sub-layer–," *Journal of Power and Energy Systems*, **6**(3), pp. 446-461 (2012).
25. K. Hata, Y. Shirai, S. Masuzaki and A. Hamura, "Computational Study of Twisted-Tape-Induced Swirl

Flow Heat Transfer and Pressure Drop in a Vertical Circular Tube under Velocities Controlled," *Nuclear Engineering and Design*, **263**, pp. 443-455 (2013).

26. K. Hata, K. Fukuda and S. Masuzaki, "Conductive Sub-layer of Turbulent Heat Transfer for Heating of Water in a Circular Tube," *Heat and Mass Transfer*, DOI: 10.1007/s00231-017-1996-5, **53**, pp. 2559-2576 (2017).
27. K. Hata, K. Fukuda and S. Masuzaki, "Conductive Sub-Layer of Twisted-Tape-Induced Swirl-Flow Heat Transfer in Vertical Circular Tubes with Various Twisted-Tape Inserts," *Heat and Mass Transfer*, DOI: 10.1007/s00231-017-2194-1, **54**, pp. 963-983 (2018).
28. Favre-Marinet, Michel, and Tardu, Sedat, "*Convective Heat Transfer*," ISTE Ltd and John Wiley & Sons, Inc., Great Britain and United States (2009).
29. Hanjalic, K., Kenjeres, S., Tummers, M.J., and Jonker, H.J.J., "*Analysis and Modeling of Physical Transport Phenomena*," Published by VSSD (2009).
30. K. Hata and N. Noda, "Turbulent Heat Transfer for Heating of Water in a Short Vertical Tube," *Journal of Power and Energy Systems*, **2**(1), pp. 318-329 (2008).
31. W. M. Rohsenow, "A Method of Correlating Heat-Transfer Data for Surface Boiling of Liquids," *Transactions of ASME*, **74**, pp. 969-976 (1952).
32. J. H. Lienhard, "Correlation of Limiting Liquid Superheat," *Chem. Eng. Science*, **31**, pp. 847-849 (1976).
33. D. D. Hall and I. Mudawar, "Ultra-high Critical Heat Flux (CHF) for Subcooled Water Flow Boiling-II: high-CHF Database and Design Equation," *International Journal of Heat and Mass Transfer*, **42**, pp. 1429-1456 (1999).
34. M. M. Shah, "Improved General Correlation for Critical Heat Flux during Upflow in Uniformly Heated Vertical Tubes," *International Journal of Heat and Fluid Flow*, **8**, pp. 326-335 (1987).
35. S. M. Ghiaasiaan, "Two-Phase Flow, Boiling, and Condensation in Conventional and Miniature Systems," Cambridge University Press, p. 381 (2008).

APPENDIX A

A.1. Relationship between the heat transfer coefficient, h, and the thickness of the average conductive

sub-layer, $\delta_{CSL,av}$, on forced convection

Figure 35 is shown typical example of the heat transfer coefficient curves (h vs. ΔT_L) for the exponential period, τ, of around 25 s on the Platinum test tube of d=3 mm and L=32.7 mm at the inlet liquid temperature, T_{in}, of around 308.38 K and the flow velocities, u, of 4 and 13.3 m/s. At a constant flow velocity, the experimental and numerical analysis results of the heat transfer coefficient are almost constant and agree within ±15 % difference, and they match the non-boiling forced convection curve derived from the correlation, Eq. (74), up to the point where the heat transfer coefficient rapidly increases with the onset of nucleate boiling.

$$h = 0.02 \frac{\lambda_l}{d} Re_d^{0.85} Pr^{0.4} \left(\frac{L}{d}\right)^{-0.08} \left(\frac{\mu}{\mu_w}\right)^{0.14} \quad (\mathrm{W/m^2K}) \quad (74)$$

All properties of the equation are evaluated at the average bulk liquid temperature, T_L, [=(T_{in}+(T_{out})$_{cal}$)/2], except μ_w, which is evaluated at the heater inner surface temperature. The heat transfer coefficient, h, is proportional to the reciprocal of the thickness of the conductive sub-layer, $1/\delta_{CSL,av}$ [26].

$$h \simeq 0.5 \frac{1}{\delta_{CSL,av}} \quad (\mathrm{W/m^2K}) \quad (75)$$

Figure and Table Captions

Fig. 1 Schematic diagram of experimental setup.

Fig. 2 Vertical cross-sectional view of 3 mm inner diameter test section.

Fig. 3 Result of SEM photograph of the inner surface of platinum (Pt) test tube of d=3 mm with the commercial finish of inner surface.

Fig. 4 Measurement and data processing system.

Fig. 5 Physical model for numerical analysis.

Table 1 The values of the constants in the Chen-Kim k-ε turbulence model [20].

Fig. 6 Liquid temperatures in the conductive sub-layer, δ_{CSL}, based on numerically predicted data points (solution of RANS equations) for d=3 mm and L=32.7 mm test tube.

Fig. 7 Typical heat transfer processes on the Pt test tube of d=3 mm and L=32.7 mm for τ=around 25 s with u=4.0, 6.9, 9.9, 13.3, 17 and 21 m/s compared with numerical solutions of inner surface temperature.

Fig. 8 Average inner surface temperature, heat flux and inlet and outlet temperatures on the Pt test tube of d=3 mm and L=32.7 mm for q=3.01 MW/m^2 with u=13.64 m/s and τ=25.27 s at the elapsed time of 138 s compared with numerical solutions of *TEM* and inner surface temperature numerically analyzed by δ_{CSL}=6.52 μm, and y^+_{CSL}, δ_{VSL}, y^+_{VSL} and Prandtl numbers evaluated at *TEM*, $(Pr)_{TEM}$, on forced convection.

Table 2 Thicknesses and nondimensional thicknesses of local conductive and viscous sub-layers, δ_{CSL}, δ_{VSL}, y^+_{CSL} and y^+_{VSL}, and Prandtl numbers evaluated at *TEM*, $(Pr)_{TEM}$, on forced convection for various T_s with q=3.01 MW/m^2.

Fig. 9 Average inner surface temperature, heat flux and inlet and outlet temperatures on the Pt test tube of d=3 mm and L=32.7 mm for q=5.18 MW/m^2 with u=13.67 m/s and τ=25.27 s at the elapsed time of 150 s compared with numerical solutions of *TEM* and inner surface temperature numerically analyzed by δ_{CSL}=6.52 μm, and y^+_{CSL}, δ_{VSL}, y^+_{VSL} and Prandtl numbers evaluated at *TEM*, $(Pr)_{TEM}$, on forced convection.

Table 3 Thicknesses and nondimensional thicknesses of local conductive and viscous sub-layers, δ_{CSL}, δ_{VSL}, y^+_{CSL} and y^+_{VSL}, and Prandtl numbers evaluated at *TEM*, $(Pr)_{TEM}$, on forced convection for various T_s with q=5.18 MW/m^2.

Fig. 10 Average inner surface temperature, heat flux and inlet and outlet temperatures on the Pt test tube of d=3 mm and L=32.7 mm for q=8.91 MW/m^2 with u=13.71 m/s and τ=25.27 s at the elapsed time of 163.2

s compared with numerical solutions of *TEM* and inner surface temperature numerically analyzed by δ_{CSL}=6.52 μm, and y^+_{CSL}, δ_{VSL}, y^+_{VSL} and Prandtl numbers evaluated at *TEM*, $(Pr)_{TEM}$, on forced convection.

Table 4 Thicknesses and nondimensional thicknesses of local conductive and viscous sub-layers, δ_{CSL}, δ_{VSL}, y^+_{CSL} and y^+_{VSL}, and Prandtl numbers evaluated at *TEM*, $(Pr)_{TEM}$, on forced convection for various T_s with q=8.91 MW/m^2.

Fig. 11 Relationship between $\delta_{CSL,av}$ and $y^+_{CSL,av}$ for turbulent heat transfer numerically solved for circular tube of d=3 mm and L=32.7 mm, and u.

Table 5 Relationship between $\delta_{CSL,av}$ and $y^+_{CSL,av}$ (ΔT_L=100 K) for turbulent heat transfer numerically solved for Pt circular tubes of d=3 mm and L=32.7, 66.5 and 100 mm, and u.

Fig. 12 Heat transfer process on the Pt test tube of d=3 mm and L=32.7 mm for τ=23.52 s with u=4.22 m/s compared with heat transfer curves numerically analyzed by $\delta_{CSL,av}$=17.1 μm, and $y^+_{CSL,av}$, $\delta_{VSL,av}$, $y^+_{VSL,av}$ and Prandtl numbers evaluated at TEM_{av}, $(Pr)_{TEM,av}$, on forced convection.

Fig. 13 The relation between Prandtl number, *Pr*, and water temperature, *T*.

Table 6 Thicknesses and nondimensional thicknesses of average conductive and viscous sub-layers, $\delta_{CSL,av}$, $\delta_{VSL,av}$, $y^+_{CSL,av}$ and $y^+_{VSL,av}$, and Prandtl numbers evaluated at TEM_{av}, $(Pr)_{TEM,av}$, on forced convection for various ΔT_L with u=4.222 m/s.

Fig. 14 Heat transfer process on the Pt test tube of d=3 mm and L=32.7 mm for τ=24.63 s with u=7.31 m/s compared with heat transfer curves numerically analyzed by $\delta_{CSL,av}$=10.59 μm, and $y^+_{CSL,av}$, $\delta_{VSL,av}$, $y^+_{VSL,av}$ and Prandtl numbers evaluated at TEM_{av}, $(Pr)_{TEM,av}$, on forced convection.

Table 7 Thicknesses and nondimensional thicknesses of average conductive and viscous sub-layers, $\delta_{CSL,av}$, $\delta_{VSL,av}$, $y^+_{CSL,av}$ and $y^+_{VSL,av}$, and Prandtl numbers evaluated at TEM_{av}, $(Pr)_{TEM,av}$, on forced convection for various ΔT_L with u=7.314 m/s.

Fig. 15 Heat transfer process on the Pt test tube of d=3 mm and L=32.7 mm for τ=24.90 s with u=10.41 m/s compared with heat transfer curves numerically analyzed by $\delta_{CSL,av}$=8.24 μm, and $y^+_{CSL,av}$, $\delta_{VSL,av}$, $y^+_{VSL,av}$ and Prandtl numbers evaluated at TEM_{av}, $(Pr)_{TEM,av}$, on forced convection.

Table 8 Thicknesses and nondimensional thicknesses of average conductive and viscous sub-layers, $\delta_{CSL,av}$, $\delta_{VSL,av}$, $y^+_{CSL,av}$ and $y^+_{VSL,av}$, and Prandtl numbers evaluated at TEM_{av}, $(Pr)_{TEM,av}$, on forced convection for various ΔT_L with u=10.407 m/s.

Fig. 16 Heat transfer process on the Pt test tube of d=3 mm and L=32.7 mm for τ=25.27 s with u=13.72 m/s compared with heat transfer curves numerically analyzed by $\delta_{CSL,av}$=6.52 μm, and $y^+_{CSL,av}$, $\delta_{VSL,av}$, $y^+_{VSL,av}$ and Prandtl numbers evaluated at TEM_{av}, $(Pr)_{TEM,av}$, on forced convection.

Table 9 Thicknesses and nondimensional thicknesses of average conductive and viscous sub-layers, $\delta_{CSL,av}$, $\delta_{VSL,av}$, $y^+_{CSL,av}$ and $y^+_{VSL,av}$, and Prandtl numbers evaluated at TEM_{av}, $(Pr)_{TEM,av}$, on forced convection for various ΔT_L with u=13.715 m/s.

Fig. 17 Heat transfer process on the Pt test tube of d=3 mm and L=32.7 mm for τ=25.16 s with u=17.34 m/s compared with heat transfer curves numerically analyzed by $\delta_{CSL,av}$=5.24 μm, and $y^+_{CSL,av}$, $\delta_{VSL,av}$, $y^+_{VSL,av}$ and Prandtl numbers evaluated at TEM_{av}, $(Pr)_{TEM,av}$, on forced convection.

Table 10 Thicknesses and nondimensional thicknesses of average conductive and viscous sub-layers, $\delta_{CSL,av}$, $\delta_{VSL,av}$, $y^+_{CSL,av}$ and $y^+_{VSL,av}$, and Prandtl numbers evaluated at TEM_{av}, $(Pr)_{TEM,av}$, on forced convection for various ΔT_L with u=17.340 m/s.

Fig. 18 Heat transfer process on the Pt test tube of d=3 mm and L=32.7 mm for τ=25.95 s with u=21.45 m/s compared with heat transfer curves numerically analyzed by $\delta_{CSL,av}$=3.48 μm, and $y^+_{CSL,av}$, $\delta_{VSL,av}$, $y^+_{VSL,av}$ and Prandtl numbers evaluated at TEM_{av}, $(Pr)_{TEM,av}$, on forced convection.

Table 11 Thicknesses and nondimensional thicknesses of average conductive and viscous sub-layers, $\delta_{CSL,av}$, $\delta_{VSL,av}$, $y^+_{CSL,av}$ and $y^+_{VSL,av}$, and Prandtl numbers evaluated at TEM_{av}, $(Pr)_{TEM,av}$, on forced convection for various ΔT_L with u=21.446 m/s.

Fig. 19 Thickness of average conductive sub-layer, $\delta_{CSL,av}$, and values of $y^+_{CSL,av}$ at ΔT_L =100 K on the Pt test tube of d=3 mm versus heated length, L, at various flow velocities.

Fig. 20 Relationship between $\delta_{VSL,av}$ and $y^+_{VSL,av}$ at ΔT_L =100 K for turbulent heat transfer numerically solved for circular tube of d=3 mm and L=32.7 mm, and u.

Fig. 21 Thickness of average viscous sub-layer, $\delta_{VSL,av}$, and values of $y^+_{VSL,av}$ at ΔT_L =100 K on the Pt test tube of d=3 mm versus heated length, L, for various flow velocities.

Table 12 Relationship between $\delta_{VSL,av}$ and $y^{+}_{VSL,av}$ a ΔT_L=100 K for turbulent heat transfer numerically solved for Pt circular tubes of d=3 mm and L=32.7, 66.5 and 100 mm, and u.

Fig. 22 Heat transfer process on the Pt test tube of d=3 mm and L=32.7 mm for τ=23.52 s with u=4.22 m/s compared with heat transfer curves numerically analyzed by $\delta_{CSL,av}$, δ=17.1 to 0.33 μm.

Fig. 23 Heat transfer process on the Pt test tube of d=3 mm and L=32.7 mm for τ=24.63 s with u=7.31 m/s compared with heat transfer curves numerically analyzed by $\delta_{CSL,av}$, δ=10.59 to 0.11 μm.

Fig. 24 Heat transfer process on the Pt test tube of d=3 mm and L=32.7 mm for τ=24.90 s with u=10.41 m/s compared with heat transfer curves numerically analyzed by $\delta_{CSL,av}$, δ=8.24 to 0.09 μm.

Fig. 25 Heat transfer process on the Pt test tube of d=3 mm and L=32.7 mm for τ=25.27 s with u=13.72 m/s compared with heat transfer curves numerically analyzed by $\delta_{CSL,av}$, δ=6.52 to 0.13 μm.

Fig. 26 Heat transfer process on the Pt test tube of d=3 mm and L=32.7 mm for τ=25.16 s with u=17.34 m/s compared with heat transfer curves numerically analyzed by $\delta_{CSL,av}$, δ=5.24 to 0.48 μm.

Fig. 27 Heat transfer process on the Pt test tube of d=3 mm and L=32.7 mm for τ=25.95 s with u=21.45 m/s compared with heat transfer curves numerically analyzed by $\delta_{CSL,av}$, δ=3.48 to 0.25 μm.

Fig. 28 Experimentally measured thicknesses of the conductive sub-layer on forced convection and nucleate boiling heat transfer, $\delta_{CSL,av}$ and δ, vs. heat flux for Pt test tube of d=3 mm and L=32.7 mm with u=4 to 21 m/s.

Fig. 29 Relationship between $\delta_{CSL,av}/\delta_{CSL,av}$, $\delta/\delta_{CSL,av}$ and Bo/Bo_{cr} for Pt test tube of d=3 mm and L=32.7 mm with u=4 to 21 m/s.

Fig. 30 $q_{cr,sub,st}$ vs. $\Delta T_{sub,out}$ for an inner diameter of 3 mm with the heated length of 32.7 mm at an outlet pressure of around 800 kPa.

Fig. 31 Ratios of CHF data for the inner diameter of 3 mm with the heated length of 32.7 mm to the values derived from the outlet CHF correlation versus $\Delta T_{sub,out}$ at outlet pressure of around 800kPa.

Fig. 32 $q_{cr,sub,st}$ vs. $\Delta T_{sub,in}$ for an inner diameter of 3 mm with the heated length of 32.7 mm at the inlet pressures of 831.51 to 942.94 kPa.

Fig. 33 Ratios of CHF data for the inner diameter of 3 mm with the heated length of 32.7 mm to the values derived from the inlet CHF correlation versus $\Delta T_{sub,in}$ at the inlet pressures of 831.51 to 942.94 kPa.

Fig. 34 Comparison of CHF data for the THD-F173 Pt test tube of d=3 mm and L=32.7 mm with the commercial finish of inner surface with authors' correlations, Eqs. (68) and (69), solutions of Celata et. al.'s liquid sub-layer dry-out model [17], Hall and Mudawar correlation, Eq. (72), [33] and Shah correlation for LCC version, Eq. (73), [34, 35].

Fig. 35 Typical heat transfer processes (h vs. ΔT_L) on the Pt test tube of d=3 mm and L=32.7 mm for τ=around 25 s with u=4.0 and 13.3 m/s compared with numerical solutions of inner surface temperature.

REFERENCES

APPENDIX A

A.1. Relationship between the heat transfer coefficient, h, and the thickness of the average conductive sub-layer, $\delta_{CSL,av}$, on forced convection

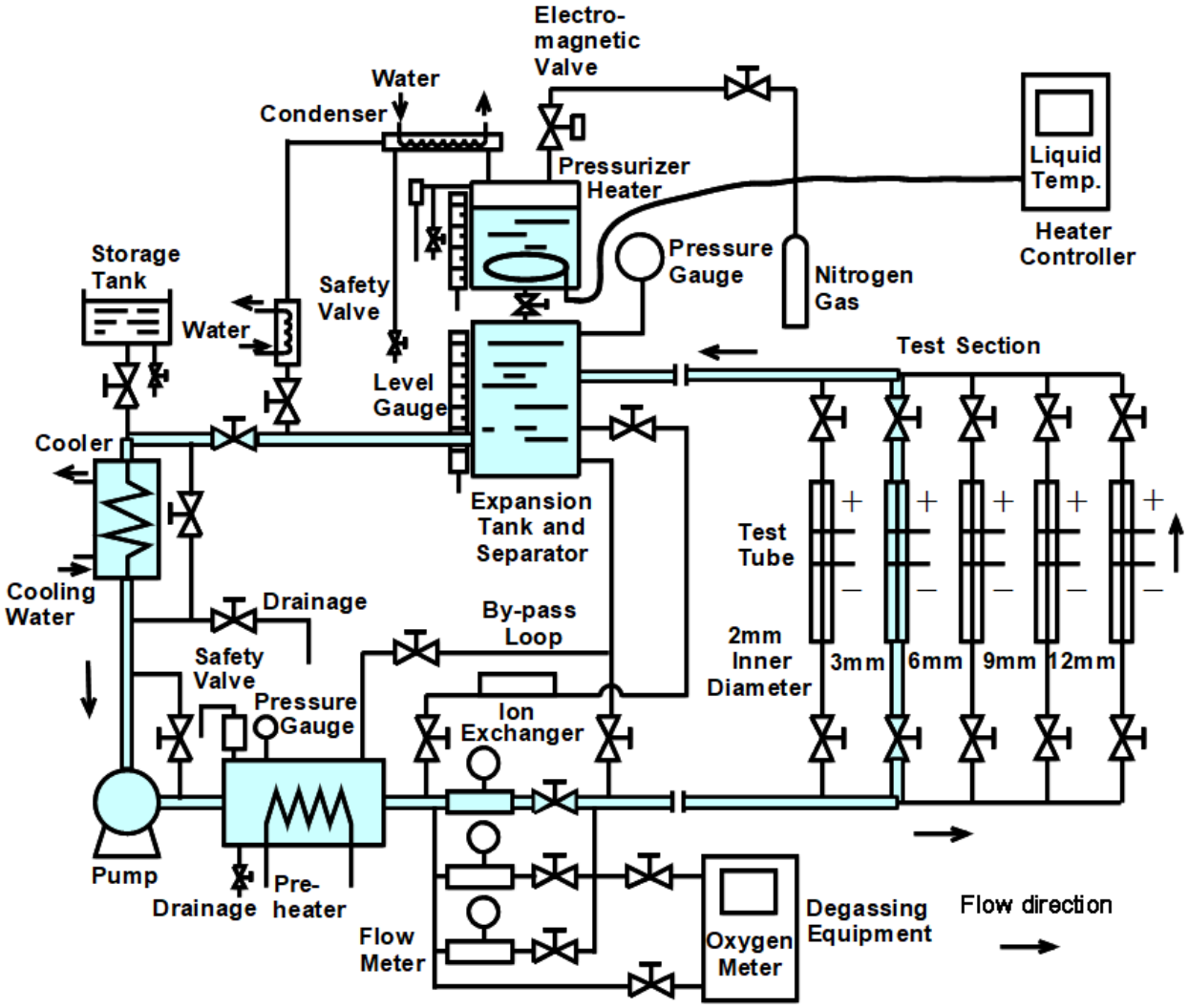

Fig. 1 Schematic diagram of experimental setup.

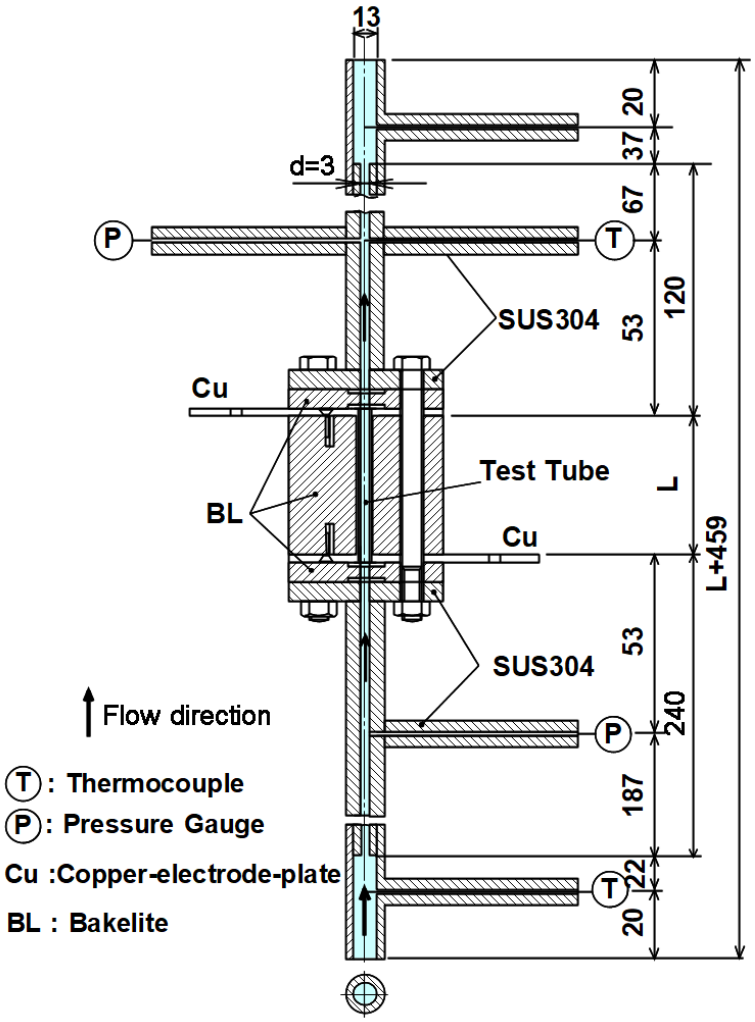

Fig. 2 Vertical cross-sectional view of the 3 mm inner diameter test section.

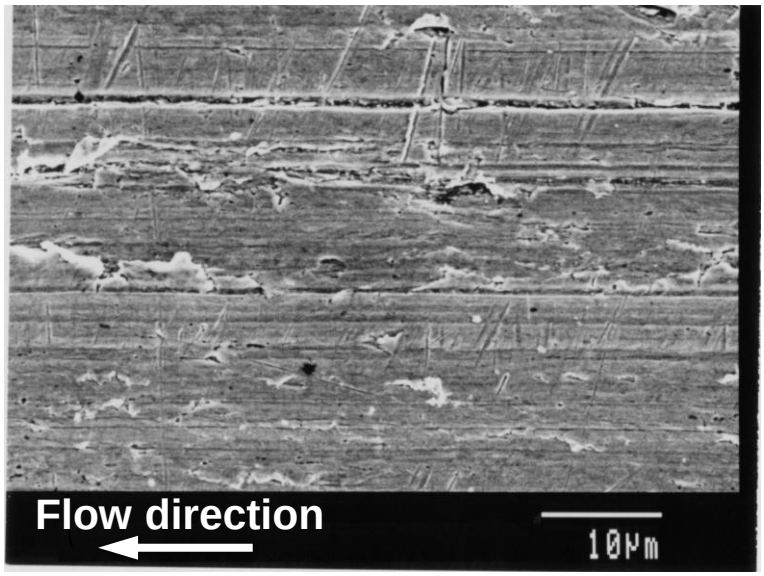

Fig. 3 Result of SEM photograph of the inner surface of platinum (Pt) test tube of d=3 mm with the commercial finish of inner surface.

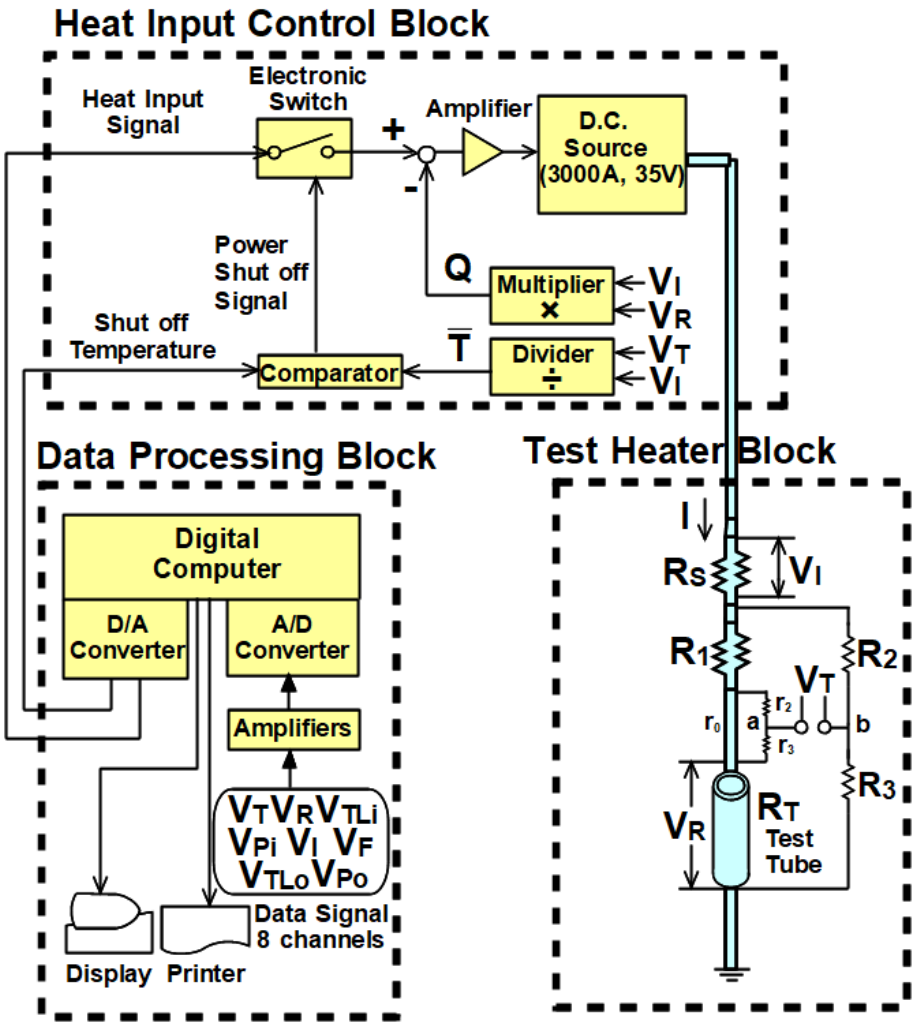

Fig. 4 Measurement and data processing system.

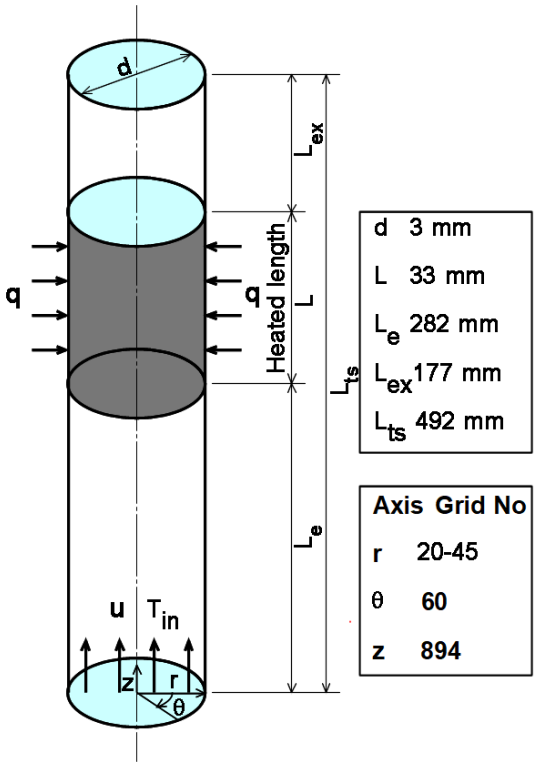

Fig. 5 Physical model for numerical analysis.

Table 1 The values of the constants in the Chen-Kim k-ε turbulence model [20].

σ_k	σ_ε	σ_t	C_{1e}	C_{2e}	C_{3e}	C_μ
0.75	1.3	1.0	1.15	1.9	0.25	0.5478

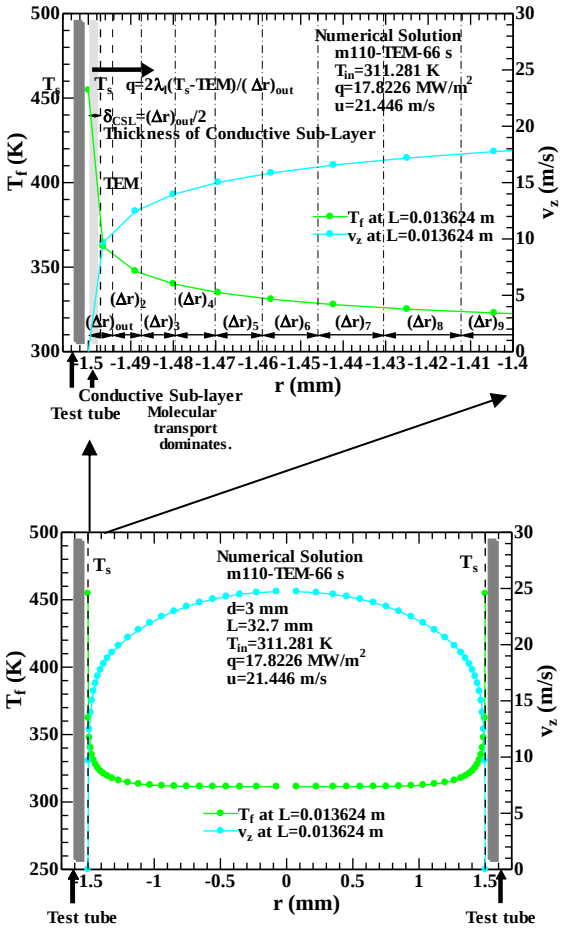

Fig. 6 Liquid temperatures in the conductive sub-layer, δ_{CSL}, based on numerically predicted data points (solution of RANS equations) for d=3 mm and L=32.7 mm test tube.

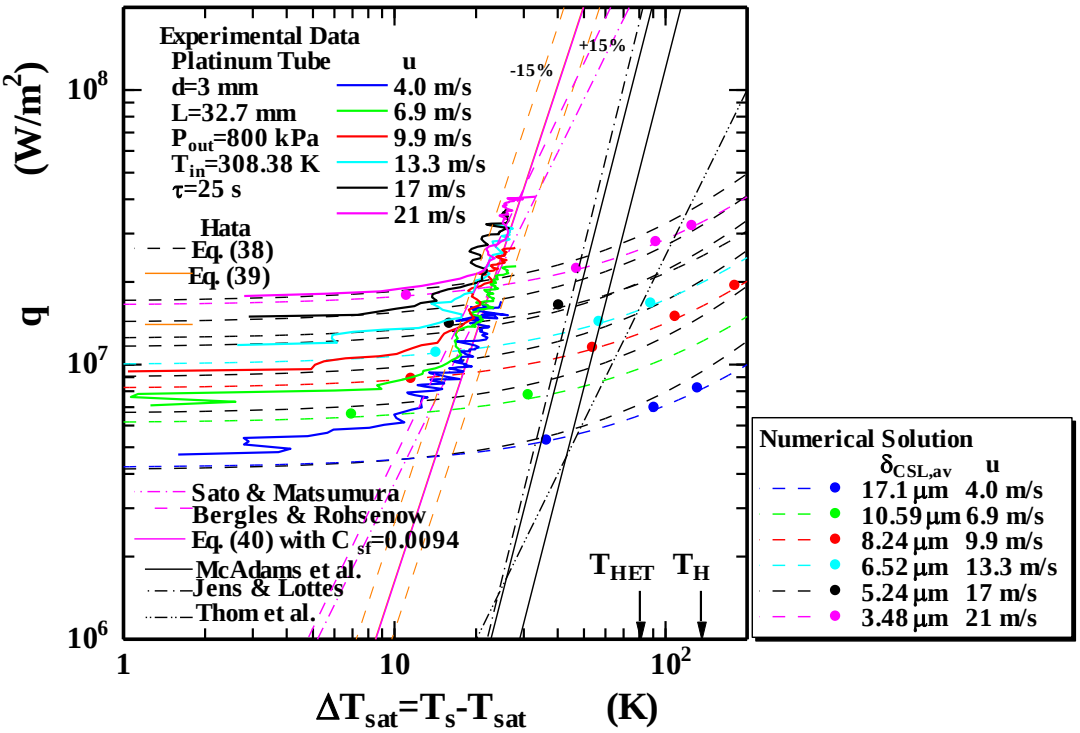

Fig. 7 Typical heat transfer processes on the Pt test tube of d=3 mm and L=32.7 mm for τ=around 25 s with u=4.0, 6.9, 9.9, 13.3, 17 and 21 m/s compared with numerical solutions of inner surface temperature.

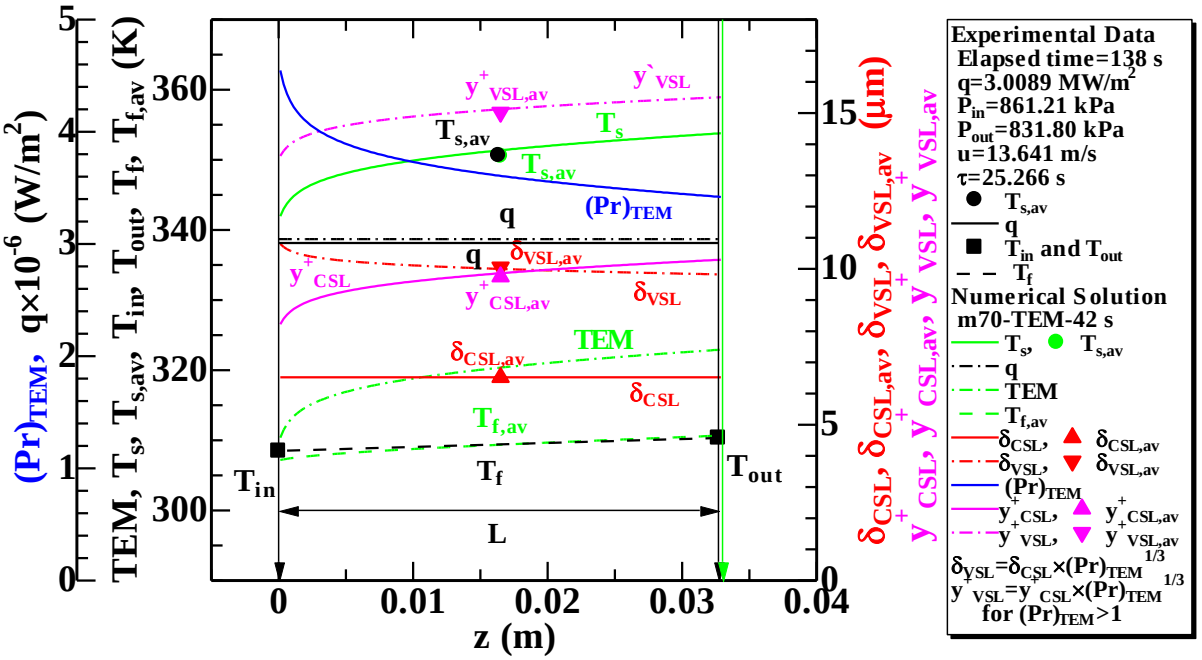

Fig. 8 Average inner surface temperature, heat flux and inlet and outlet temperatures on the Pt test tube of d=3 mm and L=32.7 mm for q=3.01 MW/m^2 with u=13.64 m/s and τ=25.27 s at the elapsed time of 138 s compared with numerical solutions of *TEM* and inner surface temperature numerically analyzed by δ_{CSL}=6.52 μm, and y^+_{CSL}, δ_{VSL}, y^+_{VSL} and Prandtl numbers evaluated at *TEM*, $(Pr)_{TEM}$, on forced convection.

Table 2 Thicknesses and nondimensional thicknesses of local conductive and viscous sub-layers, δ_{CSL}, δ_{VSL}, y^+_{CSL} and y^+_{VSL}, and Prandtl numbers evaluated at *TEM*, $(Pr)_{TEM}$, on forced convection for various T_s with q=3.01 MW/m^2.

z (mm)	0.12	4.12	8.12	12.12	16.12	20.12	24.12	28.12	32.88
T_s (K)	341.971	347.626	349.346	350.429	351.310	351.989	352.618	353.188	353.794
$(Pr)_{TEM}$	4.5466	3.9375	3.779	3.685	3.6116	3.5569	3.5076	3.4641	3.4189
δ_{CSL} (μm)	6.52	6.52	6.52	6.52	6.52	6.52	6.52	6.52	6.52
δ_{VSL} (μm)	10.8013	10.2957	10.1557	10.0707	10.0034	9.9526	9.9064	9.8653	9.8222
y^+_{CSL}	8.224	9.1995	9.5023	9.6941	9.851	9.9723	10.0851	10.1874	10.2966
y^+_{VSL}	13.6241	14.5269	14.8009	14.9735	15.1141	15.2226	15.3232	15.4144	15.5116

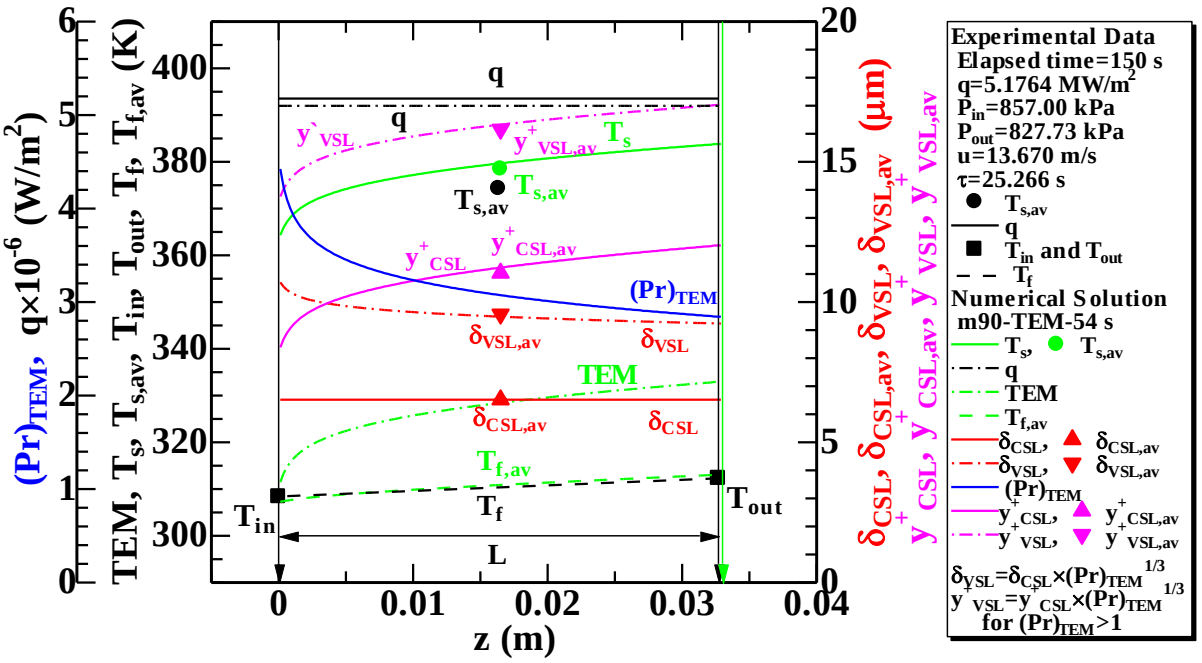

Fig. 9 Average inner surface temperature, heat flux and inlet and outlet temperatures on the Pt test tube of d=3 mm and L=32.7 mm for q=5.18 MW/m^2 with u=13.67 m/s and τ=25.27 s at the elapsed time of 150 s compared with numerical solutions of *TEM* and inner surface temperature numerically analyzed by δ_{CSL}=6.52 μm, and y^+_{CSL}, δ_{VSL}, y^+_{VSL} and Prandtl numbers evaluated at *TEM*, $(Pr)_{TEM}$, on forced convection.

Table 3 Thicknesses and nondimensional thicknesses of local conductive and viscous sub-layers, δ_{CSL}, δ_{VSL}, y^+_{CSL} and y^+_{VSL}, and Prandtl numbers evaluated at *TEM*, $(Pr)_{TEM}$, on forced convection for various T_s with q=5.18 MW/m^2.

z (mm)	0.12	4.12	8.12	12.12	16.12	20.12	24.12	28.12	32.88
T_s (K)	364.297	373.443	376.216	378.115	379.541	380.762	381.834	382.777	383.826
$(Pr)_{TEM}$	4.4238	3.5122	3.3019	3.1724	3.0821	3.0092	2.9485	2.8974	2.843
δ_{CSL} (μm)	6.52	6.52	6.52	6.52	6.52	6.52	6.52	6.52	6.52
δ_{VSL} (μm)	10.7032	9.9108	9.7089	9.5802	9.4885	9.4131	9.3493	9.295	9.2365
y^+_{CSL}	8.3845	10.0549	10.5741	10.9324	11.2028	11.4352	11.64	11.8206	12.0221
y^+_{VSL}	13.764	15.2841	15.7458	16.0635	16.3033	16.5094	16.6911	16.8516	17.031

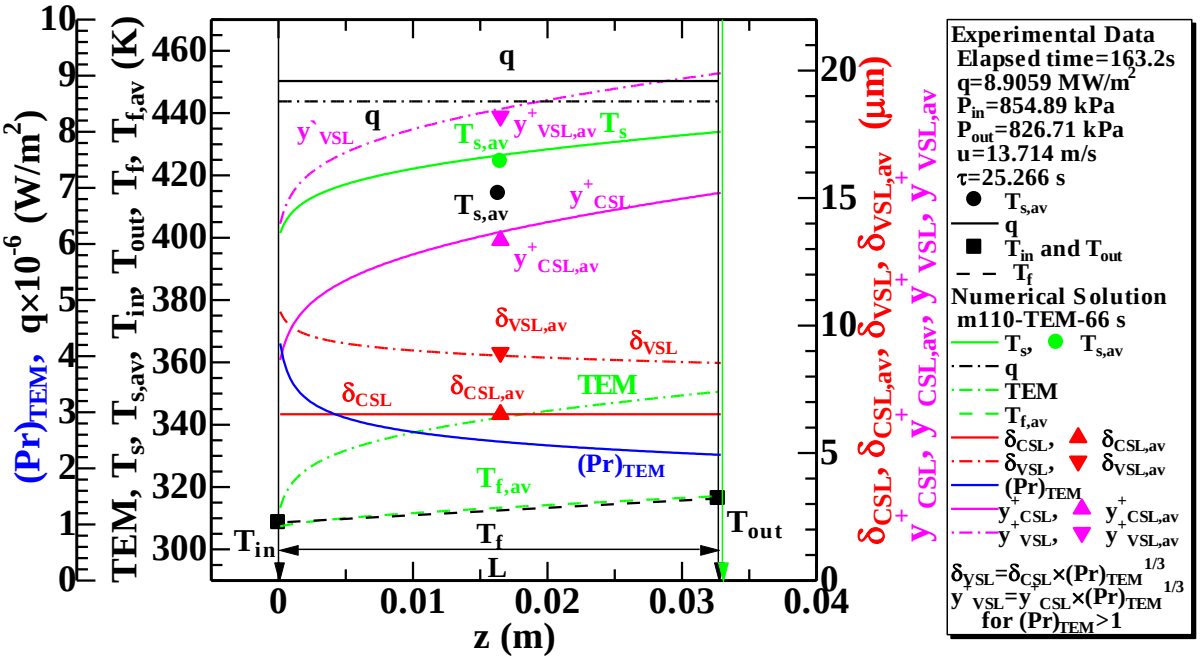

Fig. 10 Average inner surface temperature, heat flux and inlet and outlet temperatures on the Pt test tube of d=3 mm and L=32.7 mm for q=8.91 MW/m^2 with u=13.71 m/s and τ=25.27 s at the elapsed time of 163.2 s compared with numerical solutions of *TEM* and inner surface temperature numerically analyzed by δ_{CSL}=6.52 μm, and y^+_{CSL}, δ_{VSL}, y^+_{VSL} and Prandtl numbers evaluated at *TEM*, $(Pr)_{TEM}$, on forced convection.

Table 4 Thicknesses and nondimensional thicknesses of local conductive and viscous sub-layers, δ_{CSL}, δ_{VSL}, y^+_{CSL} and y^+_{VSL}, and Prandtl numbers evaluated at *TEM*, $(Pr)_{TEM}$, on forced convection for various T_s with q=8.91 MW/m^2.

z (mm)	0.12	4.12	8.12	12.12	16.12	20.12	24.12	28.12	32.88
T_s (K)	401.501	415.918	420.543	423.704	426.323	428.404	430.319	432.139	433.989
$(Pr)_{TEM}$	4.2281	2.9713	2.7236	2.5831	2.4812	2.4084	2.3469	2.2929	2.2419
δ_{CSL} (μm)	6.52	6.52	6.52	6.52	6.52	6.52	6.52	6.52	6.52
δ_{VSL} (μm)	10.5429	9.3734	9.1053	8.946	8.8268	8.7396	8.6646	8.5976	8.5334
y^+_{CSL}	8.6573	11.5249	12.4621	13.1049	13.6389	14.0632	14.454	14.8255	15.2029
y^+_{VSL}	13.9989	16.5686	17.4036	17.9811	18.4643	18.8507	19.2083	19.5496	19.8976

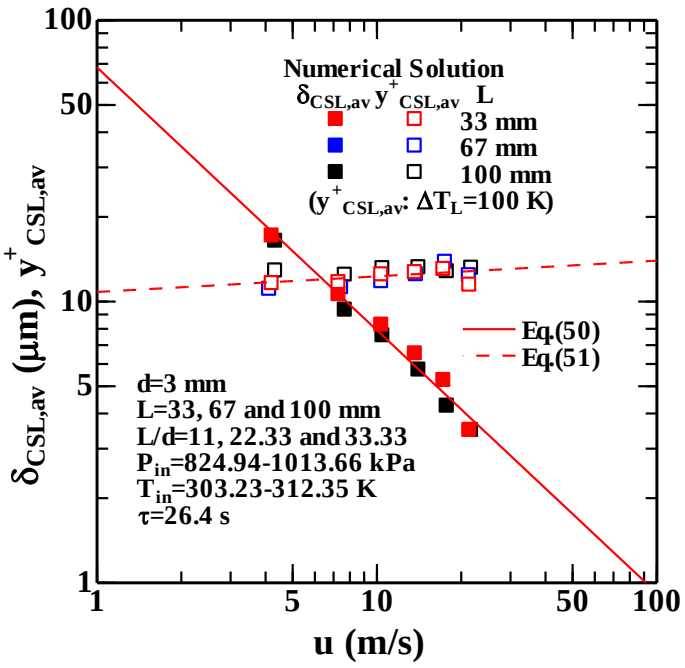

Fig. 11 Relationship between $\delta_{CSL,av}$ and $y^{+}_{CSL,av}$ for turbulent heat transfer numerically solved for circular tube of d=3 mm and L=32.7 mm, and u.

Table 5 Relationship between $\delta_{CSL,av}$ and $y^+_{CSL,av}$ (ΔT_L=100 K) for turbulent heat transfer numerically solved for Pt circular tubes of d=3 mm and L=32.7, 66.5 and 100 mm, and u.

d = 3 mm								
L = 32.7 mm			L = 66.5 mm			L = 100 mm		
u (m/s)	$\delta_{CSL,av}$ (μm)	$y^+_{CSL,av}$ (ΔT_L= 100 K)	u (m/s)	$\delta_{CSL,av}$ (μm)	$y^+_{CSL,av}$ (ΔT_L= 100 K)	u (m/s)	$\delta_{CSL,av}$ (μm)	$y^+_{CSL,av}$ (ΔT_L= 100 K)
4.222	17.1	11.58	4.14	18.1	11.05	4.343	16.38	12.85
7.314	10.59	11.68	7.47	10.35	11.20	7.713	9.32	12.41
10.407	8.24	12.44	10.40	8.01	11.76	10.497	7.56	13.09
13.715	6.52	12.67	13.83	6.52	12.46	14.123	5.71	13.19
17.340	5.24	13.00	17.57	5.24	13.79	17.833	4.25	12.77
21.446	3.48	11.43	21.39	3.48	12.36	21.787	3.48	13.14

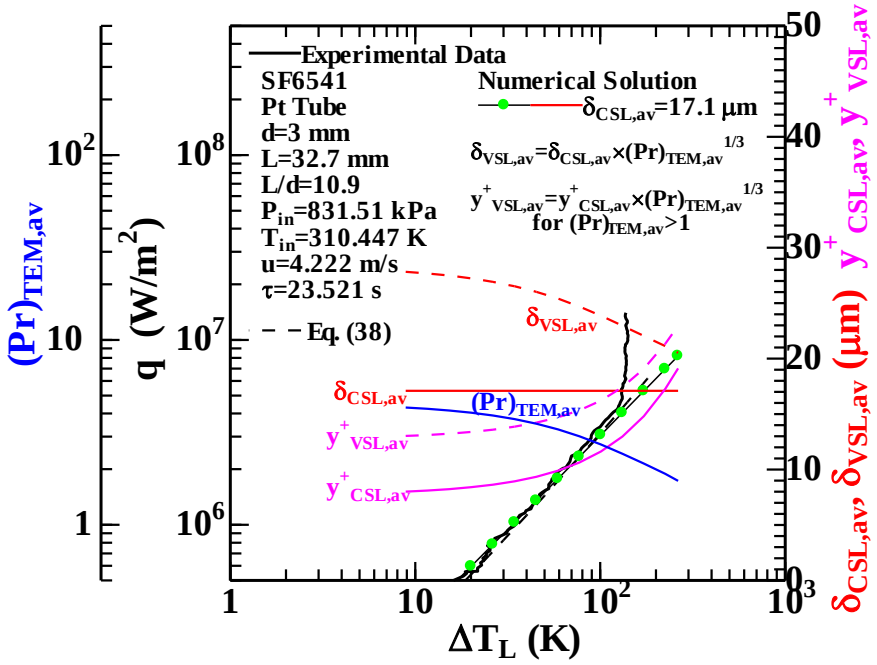

Fig. 12 Heat transfer process on the Pt test tube of d=3 mm and L=32.7 mm for τ=23.52 s with u=4.22 m/s compared with heat transfer curves numerically analyzed by $\delta_{CSL,av}$=17.1 μm, and $y^+_{CSL,av}$, $\delta_{VSL,av}$, $y^+_{VSL,av}$ and Prandtl numbers evaluated at TEM_{av}, $(Pr)_{TEM,av}$, on forced convection.

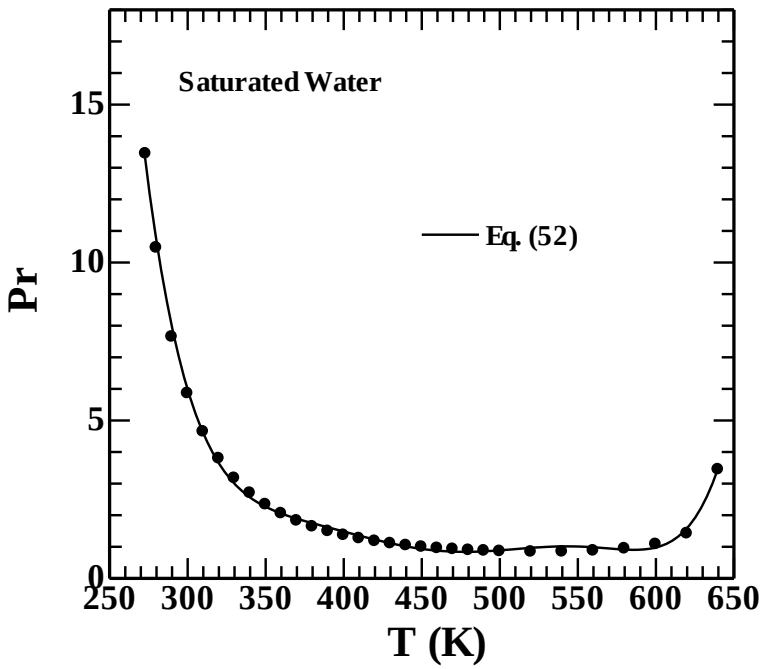

Fig. 13 The relation between Prandtl number, *Pr*, and water temperature, *T*.

Table 6 Thicknesses and nondimensional thicknesses of average conductive and viscous sub-layers, $\delta_{CSL,av}$, $\delta_{VSL,av}$, $y^+_{CSL,av}$ and $y^+_{VSL,av}$, and Prandtl numbers evaluated at TEM_{av}, $(Pr)_{TEM,av}$, on forced convection for various ΔT_L with u=4.222 m/s.

ΔT_L (K)	8.8771	20.0638	34.4825	45.1621	59.109	77.2873	100.968	171.972	263.548
$(Pr)_{TEM,av}$	4.3085	4.0407	3.7302	3.5237	3.2815	3.0088	2.7163	2.1439	1.7292
$\delta_{CSL,av}$ (μm)	17.10	17.10	17.10	17.10	17.10	17.10	17.10	17.10	17.10
$\delta_{VSL,av}$ (μm)	27.8251	27.2363	26.52	26.0214	25.4109	24.6866	23.8592	22.0495	20.5248
$y^+_{CSL,av}$	8.0047	8.407	8.9418	9.3492	9.8962	10.6314	11.626	14.8068	19.1181
$y^+_{VSL,av}$	13.0253	13.3905	13.8677	14.2269	14.7059	15.3481	16.2214	19.0926	22.9471

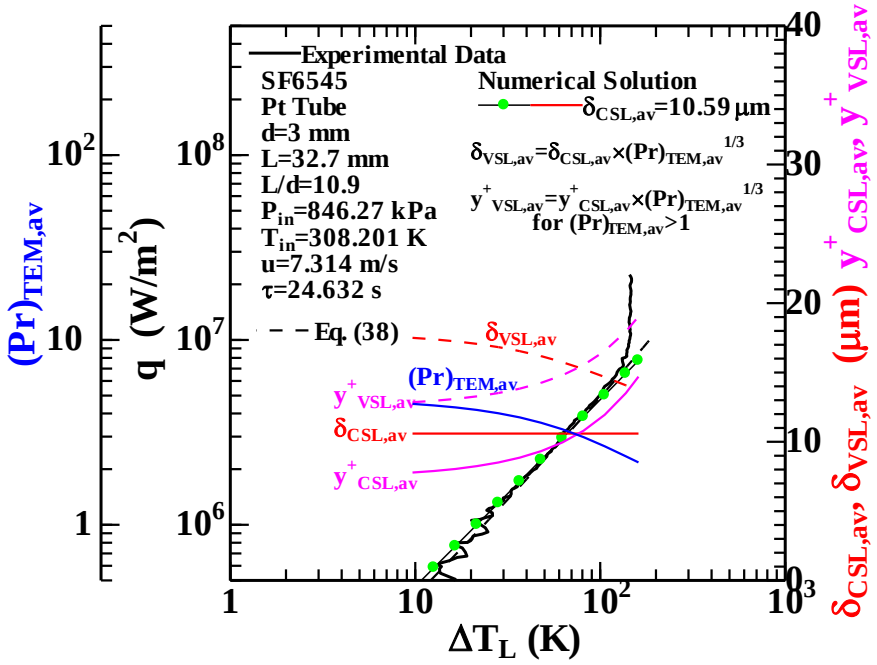

Fig. 14 Heat transfer process on the Pt test tube of d=3 mm and L=32.7 mm for τ=24.63 s with u=7.31 m/s compared with heat transfer curves numerically analyzed by $\delta_{CSL,av}$=10.59 μm, and $y^+_{CSL,av}$, $\delta_{VSL,av}$, $y^+_{VSL,av}$ and Prandtl numbers evaluated at TEM_{av}, $(Pr)_{TEM,av}$, on forced convection.

Table 7 Thicknesses and nondimensional thicknesses of average conductive and viscous sub-layers, $\delta_{CSL,av}$, $\delta_{VSL,av}$, $y^+_{CSL,av}$ and $y^+_{VSL,av}$, and Prandtl numbers evaluated at TEM_{av}, $(Pr)_{TEM,av}$, on forced convection for various ΔT_L with u=7.314 m/s.

ΔT_L (K)	9.6624	21.5579	36.731	47.9073	62.4326	81.2909	105.774	137.546	161.016
$(Pr)_{TEM,av}$	4.5099	4.1811	3.809	3.5659	3.2866	2.9792	2.6589	2.3481	2.1739
$\delta_{CSL,av}$ (μm)	10.59	10.59	10.59	10.59	10.59	10.59	10.59	10.59	10.59
$\delta_{VSL,av}$ (μm)	17.4965	17.0606	16.5387	16.1791	15.7451	15.2381	14.6712	14.0757	13.7187
$y^+_{CSL,av}$	7.7806	8.2442	8.8581	9.3268	9.9551	10.8011	11.9488	13.5071	14.6991
$y^+_{VSL,av}$	12.8549	13.2814	13.8338	14.2492	14.801	15.5418	16.5537	17.9529	19.0418

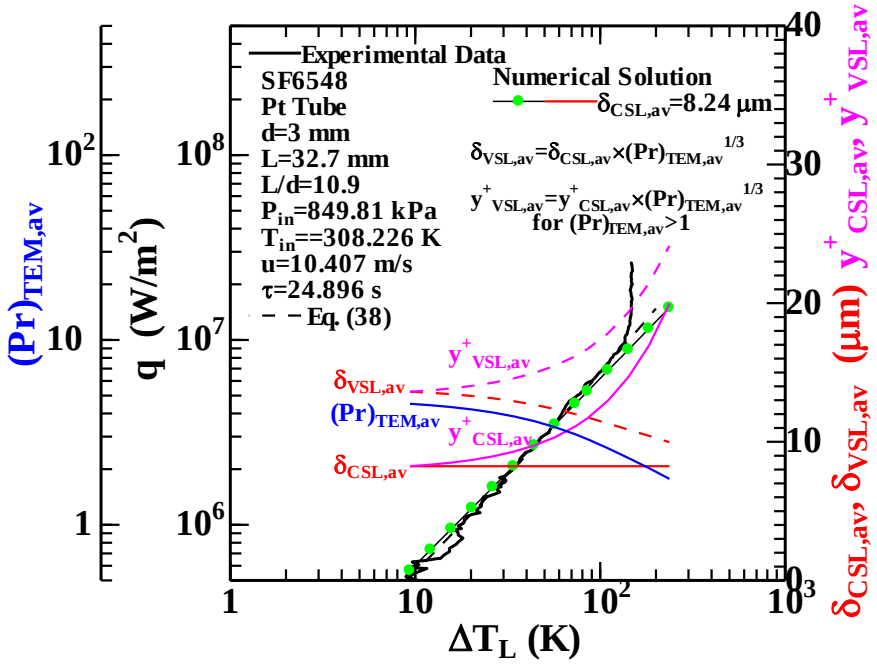

Fig. 15 Heat transfer process on the Pt test tube of d=3 mm and L=32.7 mm for τ=24.90 s with u=10.41 m/s compared with heat transfer curves numerically analyzed by $\delta_{CSL,av}$=8.24 μm, and $y^+_{CSL,av}$, $\delta_{VSL,av}$, $y^+_{VSL,av}$ and Prandtl numbers evaluated at TEM_{av}, $(Pr)_{TEM,av}$, on forced convection.

Table 8 Thicknesses and nondimensional thicknesses of average conductive and viscous sub-layers, $\delta_{CSL,av}$, $\delta_{VSL,av}$, $y^+_{CSL,av}$ and $y^+_{VSL,av}$,and Prandtl numbers evaluated at TEM_{av}, $(Pr)_{TEM,av}$, on forced convection for various ΔT_L with u=10.407 m/s.

ΔT_L (K)	9.3549	20.3269	34.0378	56.874	85.5848	110.4057	142.3623	183.4739	236.657
$(Pr)_{TEM,av}$	4.5135	4.2057	3.8608	3.3754	2.9017	2.5913	2.2939	2.0252	1.7709
δ_{CSL} (μm)	8.24	8.24	8.24	8.24	8.24	8.24	8.24	8.24	8.24
δ_{VSL} (μm)	13.6176	13.3007	12.9267	12.3605	11.7529	11.3179	10.8673	10.4252	9.9691
$y^+_{CSL,av}$	8.2378	8.6956	9.2884	10.3258	11.7124	12.9791	14.6856	16.9542	19.9446
$y^+_{VSL,av}$	13.6139	14.036	14.5713	15.4894	16.7057	17.8273	19.368	21.4504	24.1299

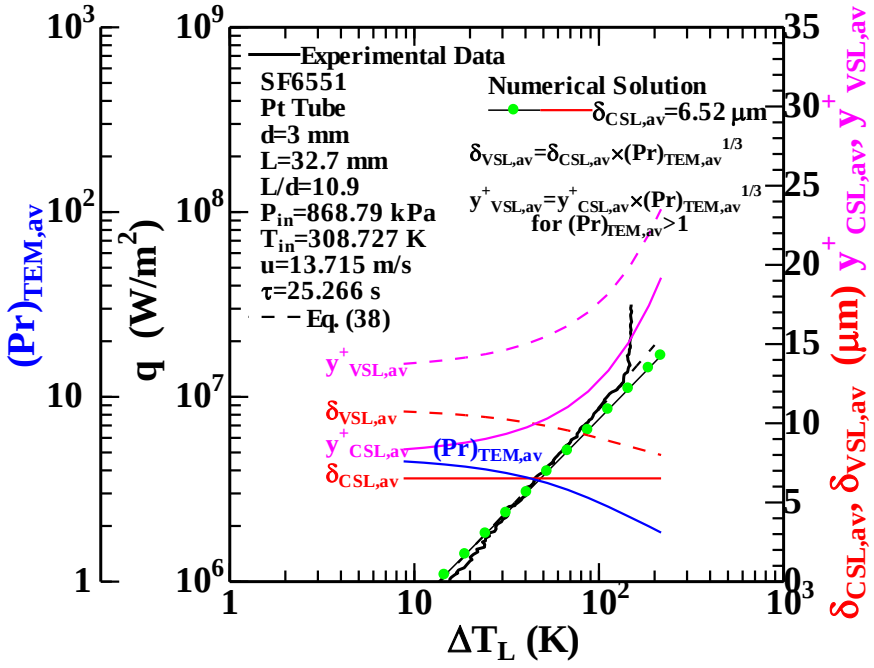

Fig. 16 Heat transfer process on the Pt test tube of d=3 mm and L=32.7 mm for τ=25.27 s with u=13.72 m/s compared with heat transfer curves numerically analyzed by $\delta_{CSL,av}$=6.52 μm, and $y^+_{CSL,av}$, $\delta_{VSL,av}$, $y^+_{VSL,av}$ and Prandtl numbers evaluated at TEM_{av}, $(Pr)_{TEM,av}$, on forced convection.

Table 9 Thicknesses and nondimensional thicknesses of average conductive and viscous sub-layers, $\delta_{CSL,av}$, $\delta_{VSL,av}$, $y^+_{CSL,av}$ and $y^+_{VSL,av}$, and Prandtl numbers evaluated at TEM_{av}, $(Pr)_{TEM,av}$, on forced convection for various ΔT_L with u=13.715 m/s.

ΔT_L (K)	8.7412	18.8952	40.7257	67.7723	87.3365	112.4952	144.8354	186.3589	216.8861
$(Pr)_{TEM,av}$	4.4738	4.1899	3.66	3.1391	2.842	2.5394	2.2515	1.9914	1.8419
$\delta_{CSL,av}$ (μm)	6.52	6.52	6.52	6.52	6.52	6.52	6.52	6.52	6.52
$\delta_{VSL,av}$ (μm)	10.743	10.5111	10.0479	9.5466	9.2354	8.8952	8.5455	8.2029	7.9923
$y^+_{CSL,av}$	8.3465	8.7768	9.747	11.0303	12.0096	13.3272	15.0969	17.4358	19.1847
$y^+_{VSL,av}$	13.753	14.1494	15.021	16.1505	17.0112	18.1823	19.7869	21.9361	23.5168

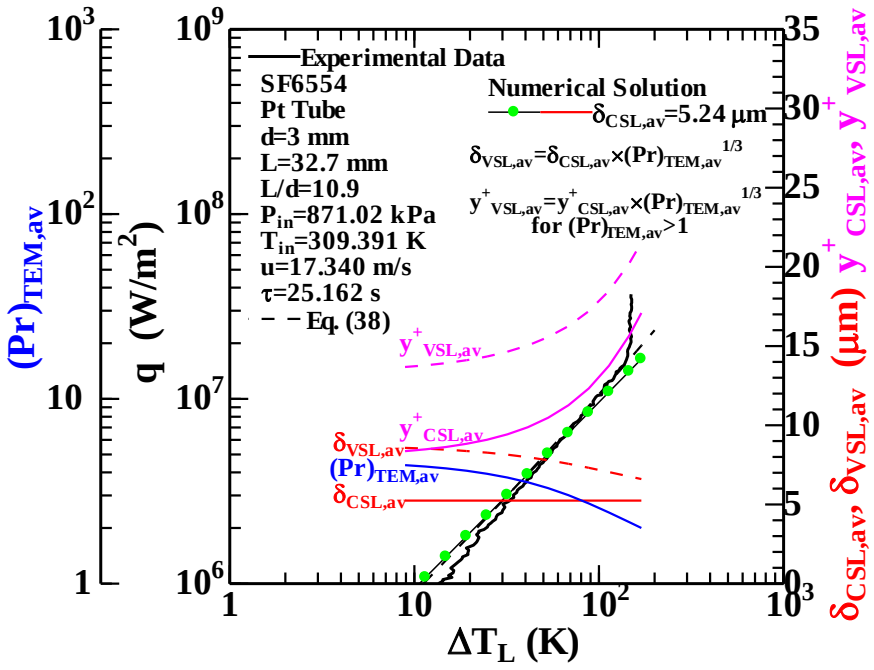

Fig. 17 Heat transfer process on the Pt test tube of d=3 mm and L=32.7 mm for τ=25.16 s with u=17.34 m/s compared with heat transfer curves numerically analyzed by $\delta_{CSL,av}$=5.24 μm, and $y^+_{CSL,av}$, $\delta_{VSL,av}$, $y^+_{VSL,av}$ and Prandtl numbers evaluated at TEM_{av}, $(Pr)_{TEM,av}$, on forced convection.

Table 10 Thicknesses and nondimensional thicknesses of average conductive and viscous sub-layers, $\delta_{CSL,av}$, $\delta_{VSL,av}$, $y^+_{CSL,av}$ and $y^+_{VSL,av}$, and Prandtl numbers evaluated at TEM_{av}, $(Pr)_{TEM,av}$, on forced convection for various ΔT_L with u=17.340 m/s.

ΔT_L (K)	8.8986	19.168	41.1738	53.0741	68.3772	88.054	113.3709	145.8645	169.629
$(Pr)_{TEM,av}$	4.378	4.0802	3.5338	3.2857	3.0099	2.7174	2.4249	2.1526	2.0017
$\delta_{CSL,av}$ (μm)	5.24	5.24	5.24	5.24	5.24	5.24	5.24	5.24	5.24
$\delta_{VSL,av}$ (μm)	8.5721	8.3732	7.9814	7.7901	7.5657	7.3123	7.0398	6.7658	6.6039
$y^+_{CSL,av}$	8.3619	8.8272	9.8758	10.4707	11.2632	12.3254	13.7574	15.6648	17.0878
$y^+_{VSL,av}$	13.6793	14.1054	15.0424	15.5664	16.2623	17.1997	18.4827	20.2261	21.5354

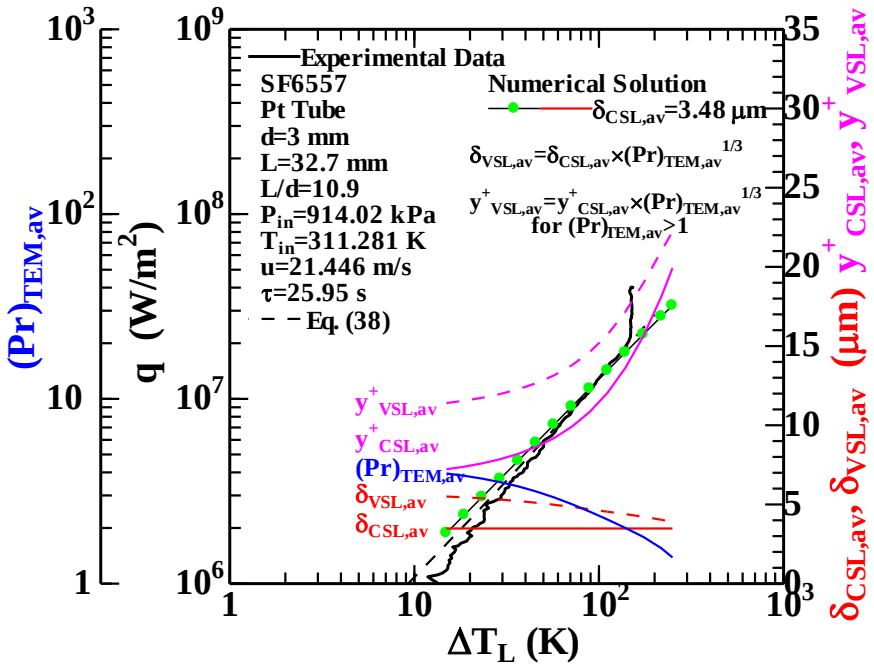

Fig. 18 Heat transfer process on the Pt test tube of d=3 mm and L=32.7 mm for τ=25.95 s with u=21.45 m/s compared with heat transfer curves numerically analyzed by $\delta_{CSL,av}$=3.48 μm, and $y^+_{CSL,av}$, $\delta_{VSL,av}$, $y^+_{VSL,av}$ and Prandtl numbers evaluated at TEM_{av}, $(Pr)_{TEM,av}$, on forced convection.

Table 11 Thicknesses and nondimensional thicknesses of average conductive and viscous sub-layers, $\delta_{CSL,av}$, $\delta_{VSL,av}$, $y^+_{CSL,av}$ and $y^+_{VSL,av}$, and Prandtl numbers evaluated at TEM_{av}, $(Pr)_{TEM,av}$, on forced convection for various ΔT_L with u=21.446 m/s.

ΔT_L (K)	14.9183	29.1945	45.6221	71.2104	111.1483	138.9803	173.899	217.9148	249.9649
$(Pr)_{TEM,av}$	3.9454	3.5406	3.154	2.6933	2.2221	2.0032	1.7898	1.5534	1.3857
$\delta_{CSL,av}$ (μm)	3.48	3.48	3.48	3.48	3.48	3.48	3.48	3.48	3.48
$\delta_{VSL,av}$ (μm)	5.4989	5.304	5.1035	4.8418	4.5412	4.3869	4.2252	4.0303	3.8797
$y^+_{CSL,av}$	7.2174	7.8567	8.6295	9.9046	12.0442	13.6154	15.6242	18.1409	19.9283
$y^+_{VSL,av}$	11.4045	11.9747	12.6553	13.7806	15.7168	17.1635	18.9699	21.0098	22.2172

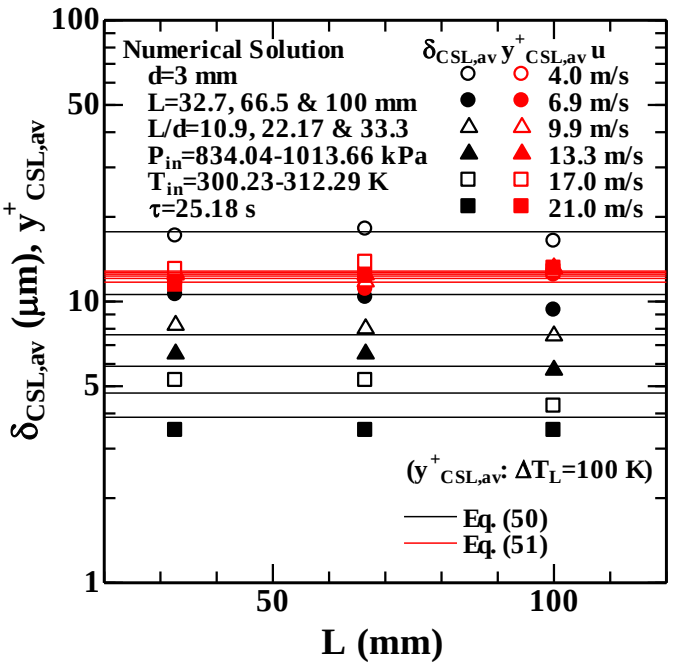

Fig. 19 Thickness of average conductive sub-layer, $\delta_{CSL,av}$, and values of $y^+_{CSL,av}$ at ΔT_L =100 K on the Pt test tube of d=3 mm versus heated length, L, for various flow velocities.

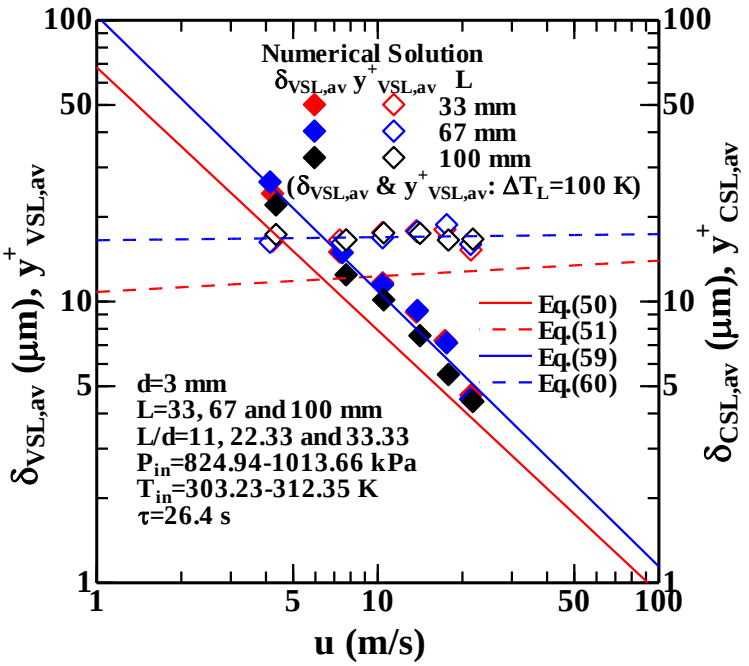

Fig. 20 Relationship between $\delta_{VSL,av}$ and $y^{+}_{VSL,av}$ at ΔT_L =100 K for turbulent heat transfer numerically solved for circular tube of d=3 mm and L=32.7 mm, and u.

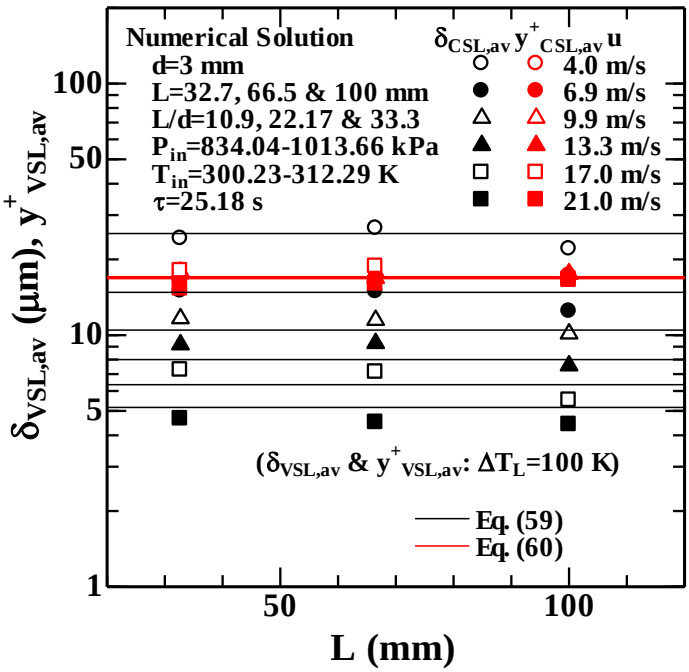

Fig. 21 Thickness of average viscous sub-layer, $\delta_{VSL,av}$, and values of $y^+_{VSL,av}$ at ΔT_L =100 K on the Pt test tube of d=3 mm versus heated length, L, for various flow velocities.

Table 12 Relationship between $\delta_{VSL,av}$ and $y^+_{VSL,av}$ a ΔT_L=100 K for turbulent heat transfer numerically solved for Pt circular tubes of d=3 mm and L=32.7, 66.5 and 100 mm, and u.

d = 3 mm								
L = 32.7 mm			L = 66.5 mm			L = 100 mm		
u (m/s)	$\delta_{VSL,av}$ (μm) (ΔT_L= 100 K)	$y^+_{VSL,av}$ (ΔT_L= 100 K)	u (m/s)	$\delta_{VSL,av}$ (μm) (ΔT_L= 100 K)	$y^+_{VSL,av}$ (ΔT_L= 100 K)	u (m/s)	$\delta_{VSL,av}$ (μm) (ΔT_L= 100 K)	$y^+_{VSL,av}$ (ΔT_L= 100 K)
4.222	24.230193	16.408516	4.14	26.633434	16.259638	4.343	22.063833	17.308929
7.314	15.005716	16.550213	7.47	14.922306	16.147809	7.713	12.45392	16.582955
10.407	11.65116	17.589857	10.40	11.477485	16.85084	10.497	10.135865	17.550062
13.715	9.1809171	17.840831	13.83	9.2871019	17.748051	14.123	7.568781	17.483751
17.340	7.267637	18.030397	17.57	7.1335171	18.77313	17.833	5.5056522	16.542866
21.446	4.650176	15.273423	21.39	4.4991537	15.979753	21.787	4.4135627	16.665004

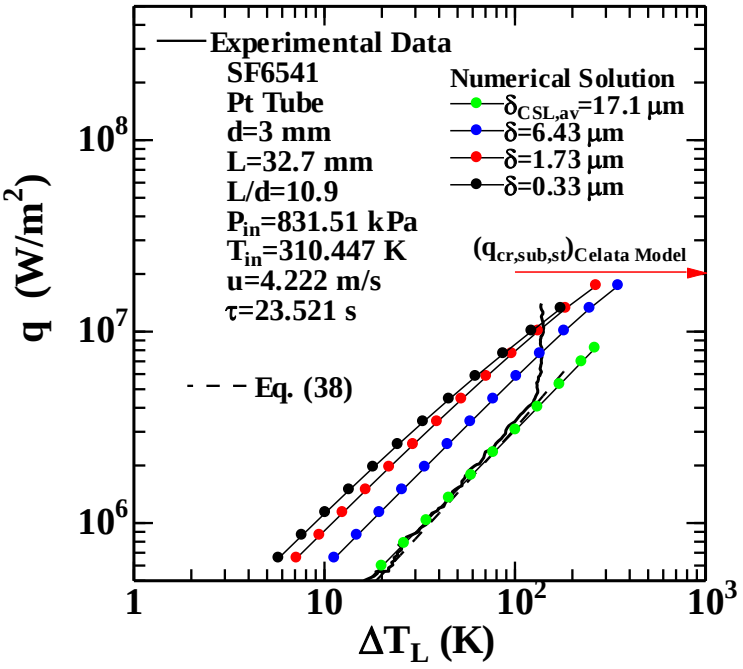

Fig. 22 Heat transfer process on the Pt test tube of d=3 mm and L=32.7 mm for τ=23.52 s with u=4.22 m/s compared with heat transfer curves numerically analyzed by $\delta_{CSL,av}$, δ=17.1 to 0.33 μm.

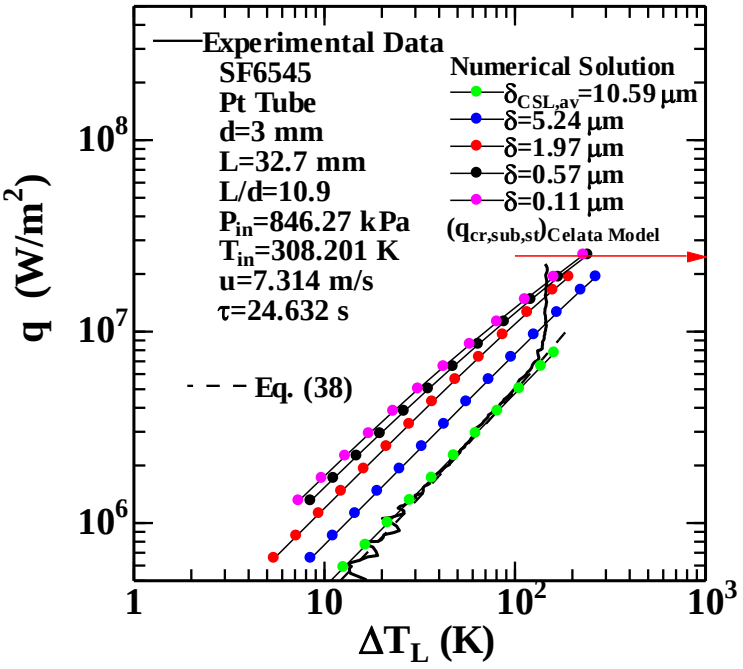

Fig. 23 Heat transfer process on the Pt test tube of d=3 mm and L=32.7 mm for τ=24.63 s with u=7.31 m/s compared with heat transfer curves numerically analyzed by $\delta_{CSL,av}$, δ=10.59 to 0.11 μm.

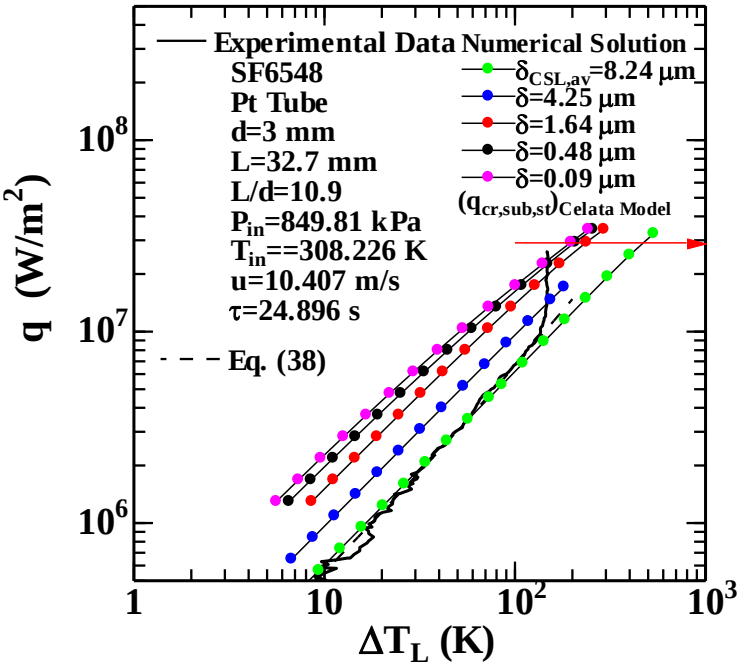

Fig. 24 Heat transfer process on the Pt test tube of d=3 mm and L=32.7 mm for τ=24.90 s with u=10.41 m/s compared with heat transfer curves numerically analyzed by $\delta_{CSL,av}$, δ=8.24 to 0.09 μm.

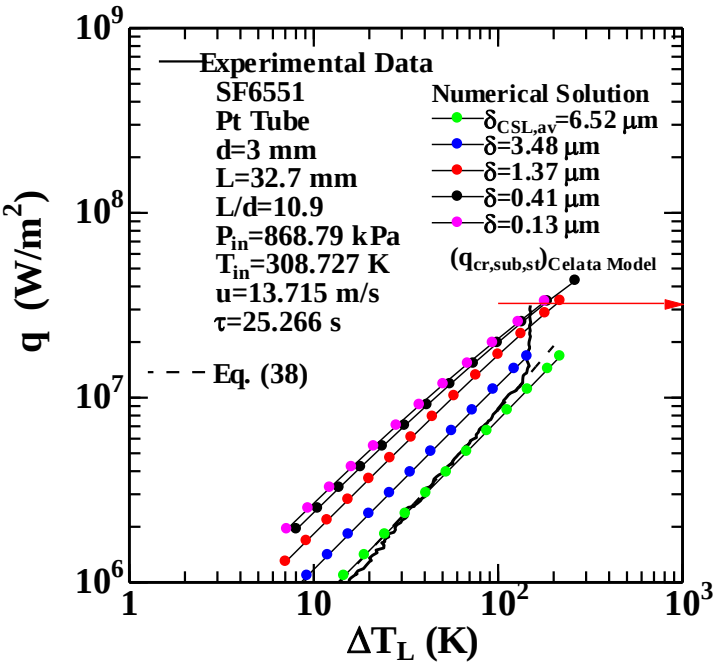

Fig. 25 Heat transfer process on the Pt test tube of d=3 mm and L=32.7 mm for τ=25.27 s with u=13.72 m/s compared with heat transfer curves numerically analyzed by $\delta_{CSL,av}$, δ=6.52 to 0.13 μm.

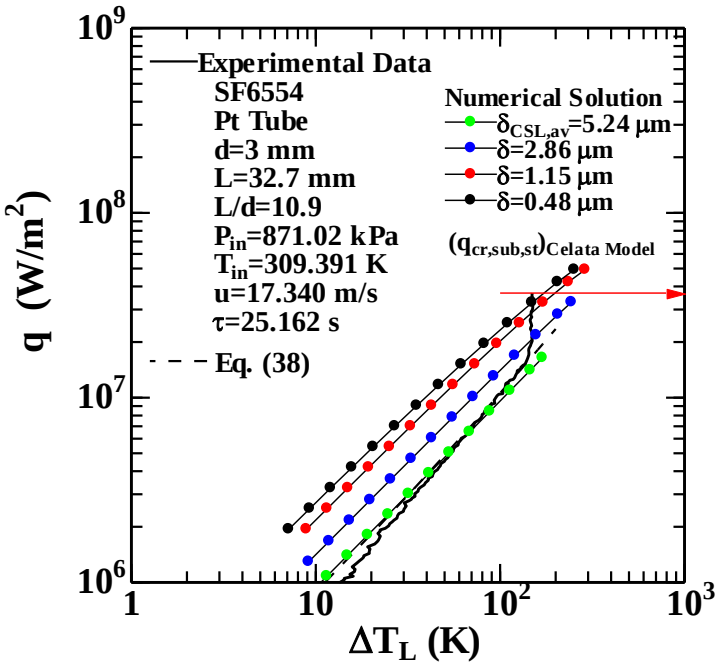

Fig. 26 Heat transfer process on the Pt test tube of d=3 mm and L=32.7 mm for τ=25.16 s with u=17.34 m/s compared with heat transfer curves numerically analyzed by $\delta_{CSL,av}$, δ=5.24 to 0.48 μm.

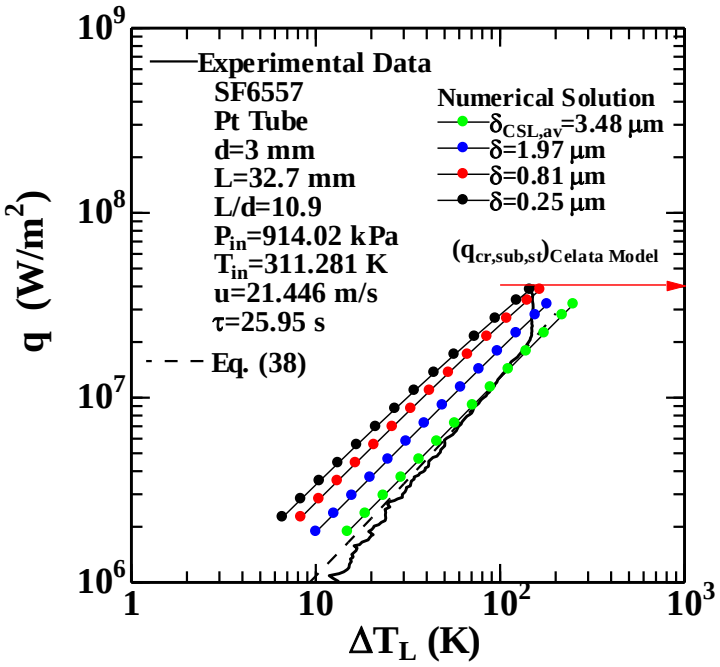

Fig. 27 Heat transfer process on the Pt test tube of d=3 mm and L=32.7 mm for τ=25.95 s with u=21.45 m/s compared with heat transfer curves numerically analyzed by $\delta_{CSL,av}$, δ=3.48 to 0.25 μm.

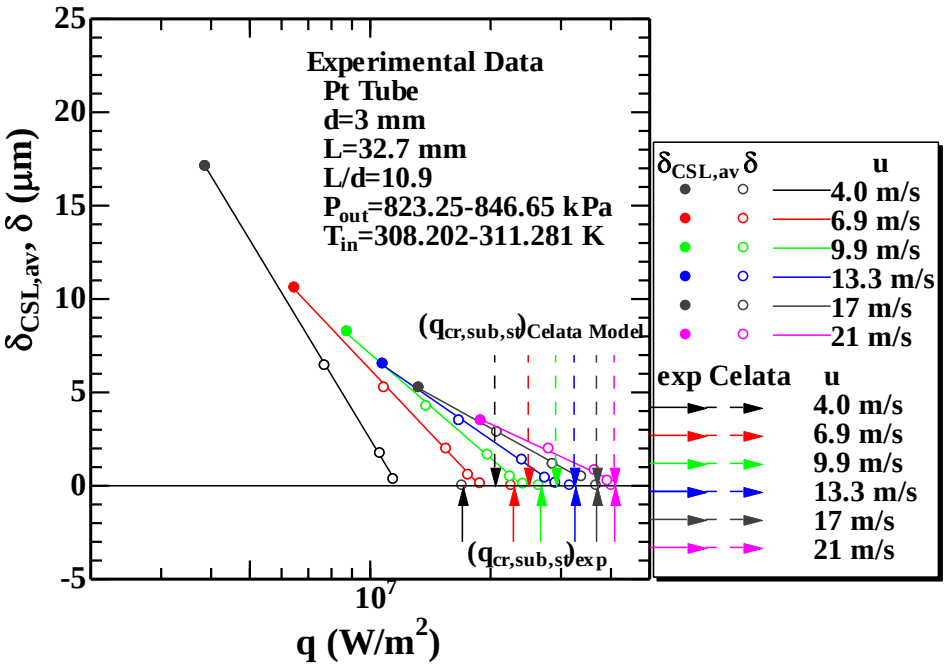

Fig. 28 Experimentally measured thicknesses of the conductive sub-layer on forced convection and nucleate boiling heat transfer, $\delta_{CSL,av}$ and δ, vs. heat flux for Pt test tube of d=3 mm and L=32.7 mm with u=4 to 21 m/s.

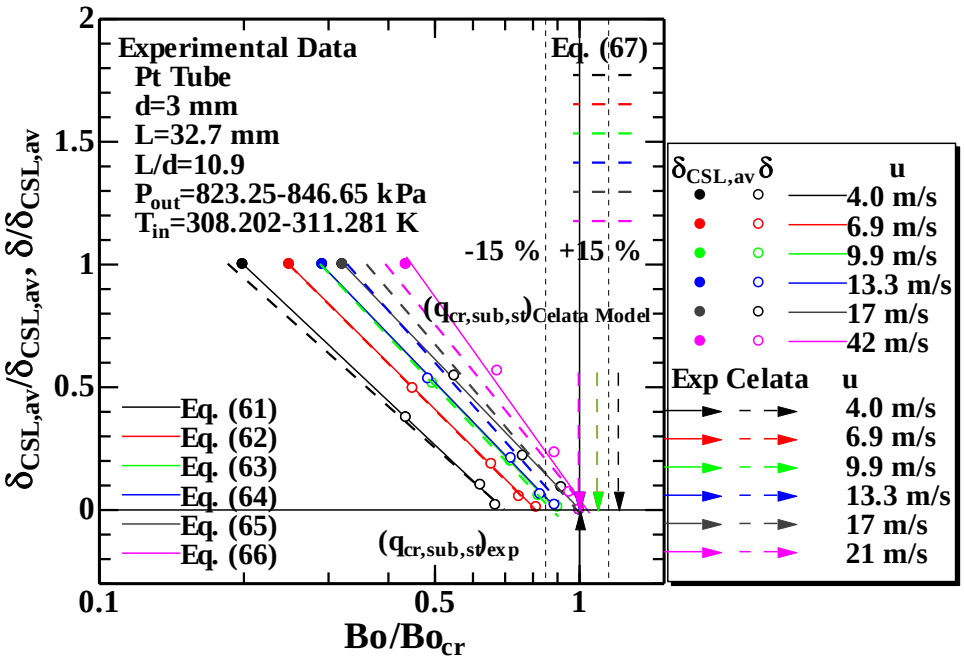

Fig. 29 Relationship between $\delta_{CSL,av}/\delta_{CSL,av}$, $\delta/\delta_{CSL,av}$ and Bo/Bo_{cr} for Pt test tube of d=3 mm and L=32.7 mm with u=4 to 21 m/s.

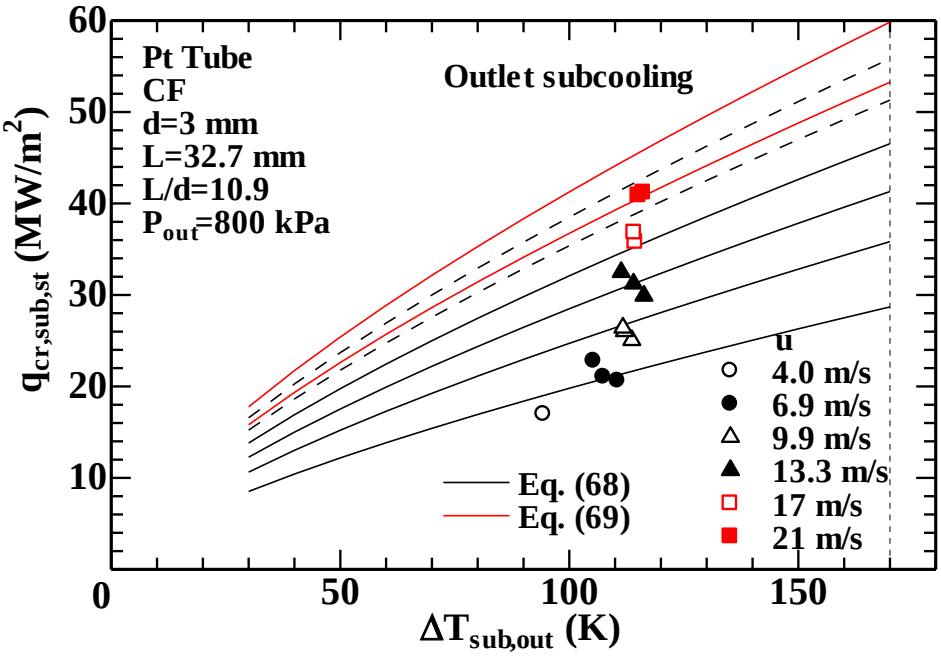

Fig. 30 $q_{cr,sub,st}$ vs. $\Delta T_{sub,out}$ for an inner diameter of 3 mm with the heated length of 32.7 mm at an outlet pressure of around 800 kPa.

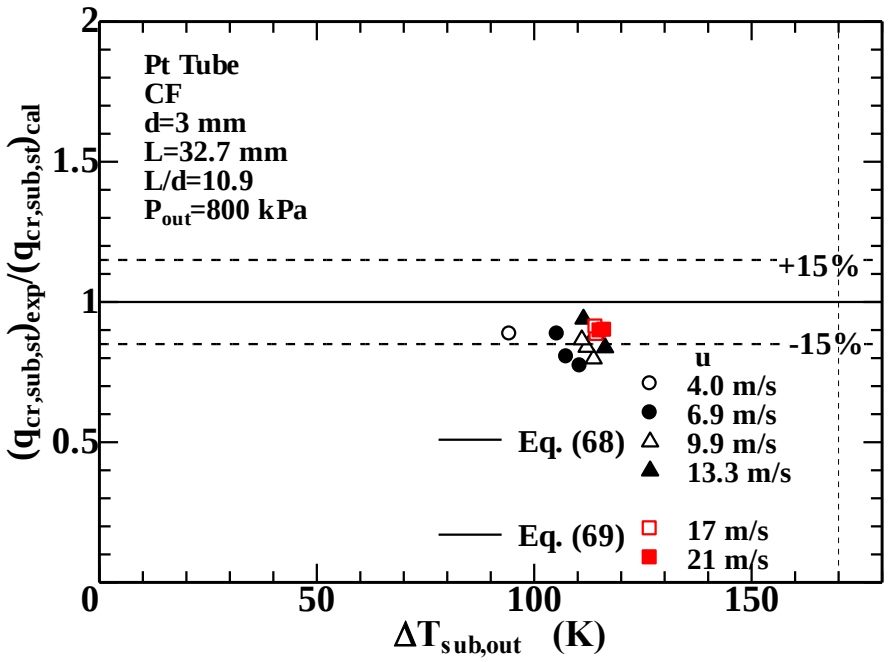

Fig. 31 Ratios of CHF data for the inner diameter of 3 mm with the heated length of 32.7 mm to the values derived from the outlet CHF correlation versus $\Delta T_{sub,out}$ at outlet pressure of around 800kPa.

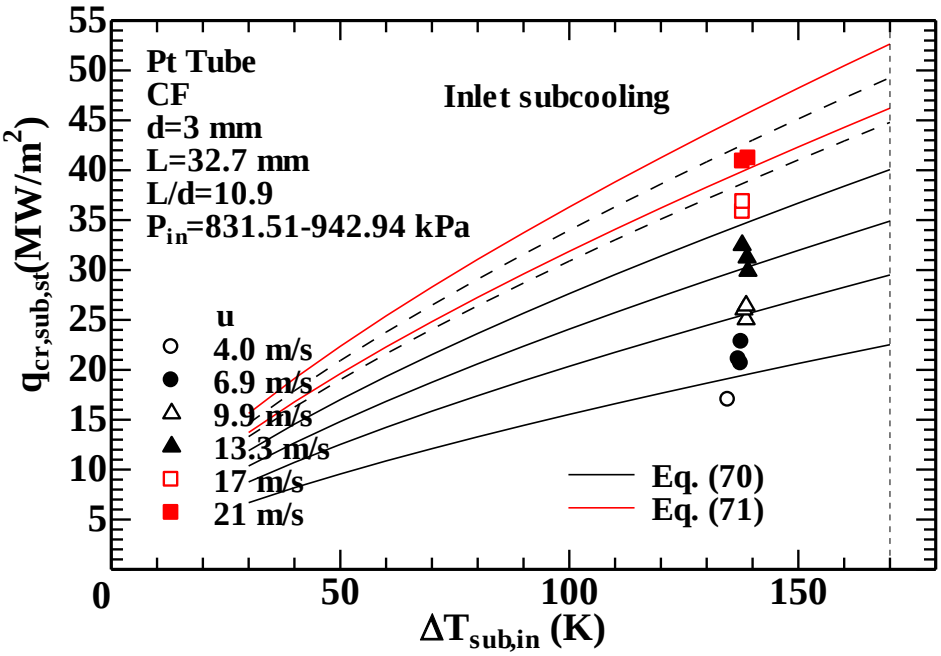

Fig. 32 $q_{cr,sub,st}$ vs. $\Delta T_{sub,in}$ for an inner diameter of 3 mm with the heated length of 32.7 mm at the inlet pressures of 831.51 to 942.94 kPa.

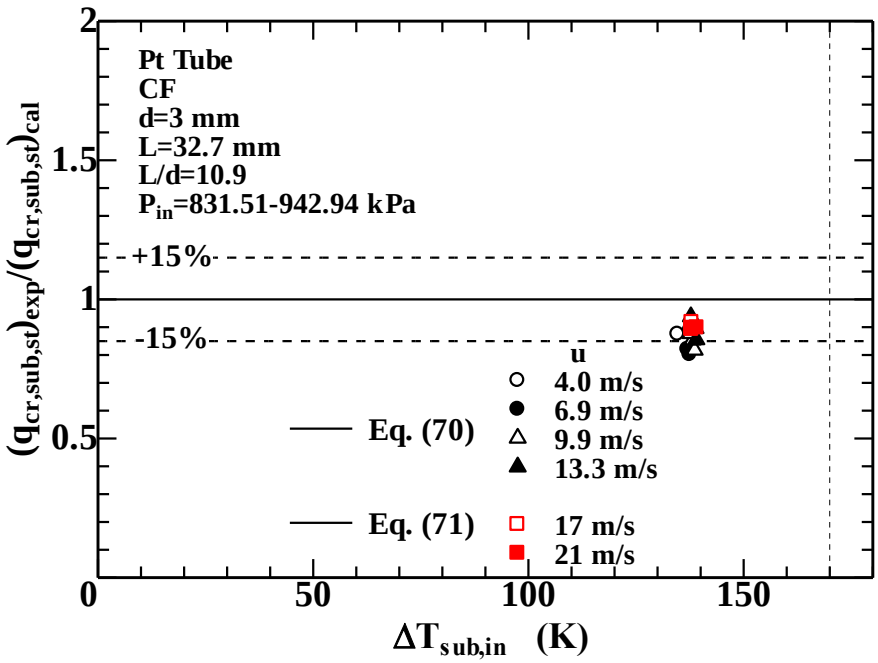

Fig. 33 Ratios of CHF data for the inner diameter of 3 mm with the heated length of 32.7 mm to the values derived from the inlet CHF correlation versus $\Delta T_{sub,in}$ at the inlet pressures of 831.51 to 942.94 kPa.

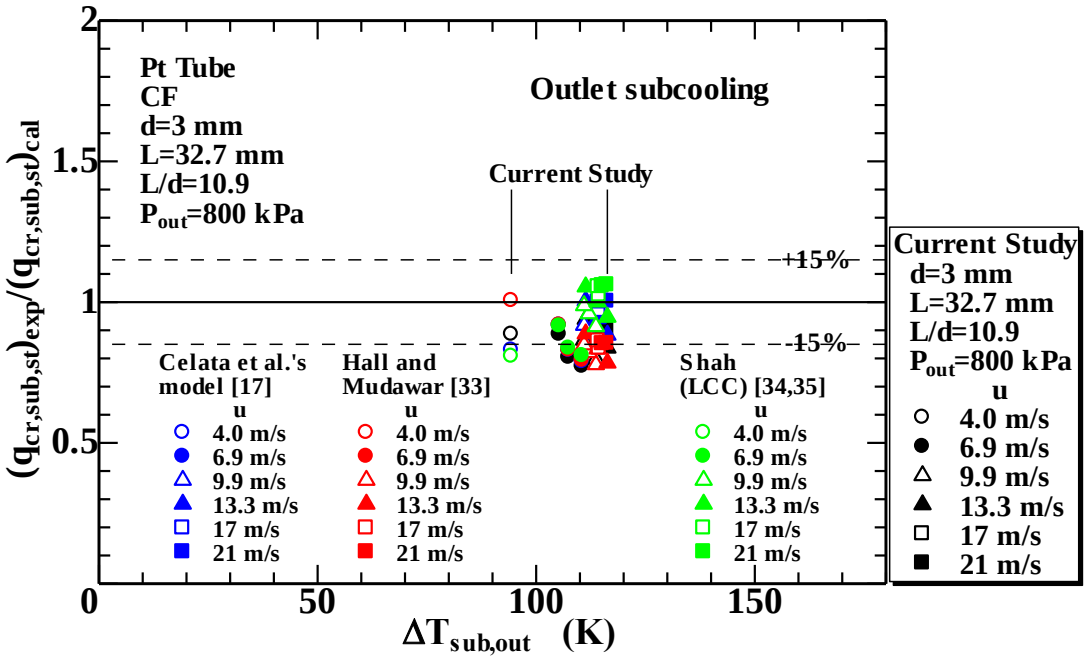

Fig. 34 Comparison of CHF data for the THD-F173 Pt test tube of *d*=3 mm and *L*=32.7 mm with the commercial finish of inner surface with authors' correlations, Eqs. (68) and (69), solutions of Celata et. al.'s liquid sub-layer dry-out model [17], Hall and Mudawar correlation, Eq. (72), [33] and Shah correlation for LCC version, Eq. (73), [34, 35].

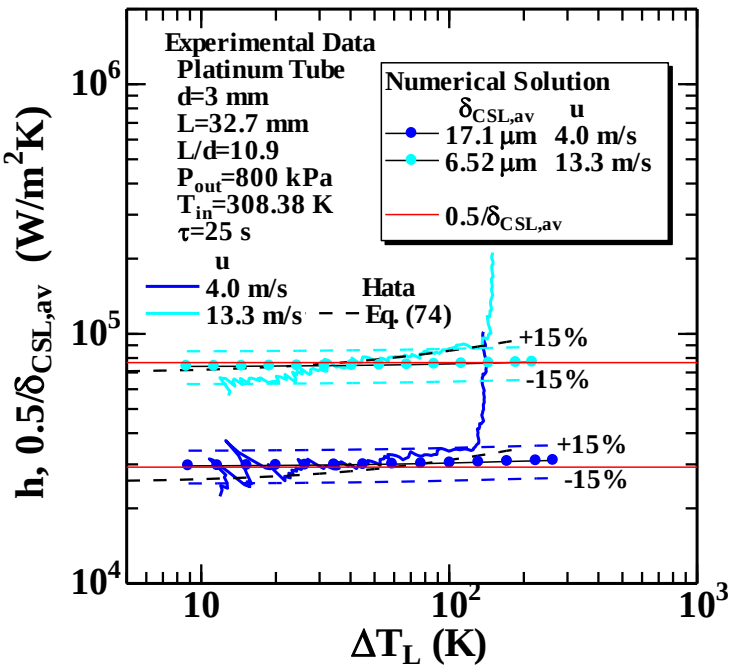

Fig. 35 Typical heat transfer processes (h vs. ΔT_L) on the Pt test tube of d=3 mm and L=32.7 mm for τ=around 25 s with u=4.0 and 13.3 m/s compared with numerical solutions of inner surface temperature.